2011 Human Powered Vehicle: Mjölnir

Portland State University Mechanical Engineering Department
1930 S.W. 4th Ave Portland, OR 97201
(503)725-4290

ME 493 Final Report - Year 2011

June 6, 2011

Team Members:
Tad Bamford
Ben Higgins
Neal Pang
Chris Schultz
Aaron Stanton
Academic Advisor:
Dr. Derek Tretheway

Sponsored By:

Executive Summary

The goal of the 2011 Portland State University (PSU) Human Powered Vehicle (HPV) team was to win the Unlimited Class Category of the 2011 American Society of Mechanical Engineers (ASME) Human Powered Vehicle Challenge (HPVC) by designing and building a race quality HPV. The competition and rules require the HPV to excel in speed, handling, reliability, efficiency, practicality and safety. With this in mind, external and internal research provided the information and ideas to formulate our detailed designs to achieve these qualities.

The final design, Mjölnir, is a leaning three wheel tadpole style recumbent tricycle with heavily dished carbon-fiber front wheels, wood leaf spring front suspension, and a partial fairing. The ability of the rider to lean into a turn gives him/her the ability to shift the center of gravity of the vehicle, increasing the top cornering speed before roll-over is initiated. The dished carbon wheels, also referred to as hub-centered wheels, are employed to locate the steering pivot axis in the center plane of the wheel to give the vehicle more stability and more efficient steering geometry. Wood leaf springs provide a zero-moving-part suspension to increase comfort and control for rough conditions and obstacles such as speed bumps.

Extensive analysis was performed to optimize the design and insure its safety. Tests were also conducted on parts and materials to gain material data and to validate analyses and computer models. Unfortunately, final design validation by racing the vehicle in competition was somewhat inconclusive because a crash in the first event disabled the vehicle and it was not ridden to its full potential. Nonetheless, most design goals were met and valuable information was gained from the accident.

Table of Contents

[1] Introduction

The fuel consumption associated with transportation needs is clearly an issue that is known throughout the world. The world's dependence on petroleum based fuels need to undergo a transformation into alternative fuel sources and a new means of transportation itself. This project is a way to design and test a vehicle that is a practical and efficient human powered vehicle that potentially will serve as a partial solution to these problems. The goal of the 2011 Portland State University (PSU) HPV team was to win the Unlimited Class Category of the 2011 Association of Mechanical Engineers (ASME) Human Powered Vehicle Challenge (HPVC) by designing and building a race quality HPV. Each year the ASME sponsors the HPVC at a chosen hosting university. This competition encourages university teams from across the United States and even the world to build and race a vehicle that moves away from the conventional upright bicycle. The vehicle should solely depend on human propulsion. It should also overcome problems in comfort, aerodynamic drag, and power efficiency associated with the traditional upright bicycle. Events of the HPVC test the speed, endurance, utility, and design of the HPVs. This year's speed event was a sprint in which the vehicle was allowed to gain speed for 500 meters before a 100 meter time trap. The speed event was scored based on the fastest time a HPV traveled the 100 meters. The two endurance events, speed and utility, were 2.5 hour relay races scored based on the number of laps completed within that time. The utility endurance event also included obstacles such as package pickup and delivery, speed bumps, a slalom section, simulated rain and complete stops. The design event score is based on a written documentation of the design process of the HPV. The goal of the following report is to show through the design process and subsequent analysis how the team sought to develop a machine that would best overcome these challenges.

[2] Goals and Design Requirements

PSU HPV has a strong recent history in the HPVC, with podium finishes in four of the last five western US competitions. This allowed design goals to be developed primarily based on the strengths and weaknesses of previous PSU designs and competition experience. Also taken into account were the HPVC rules, preferences of the design/race team and requirements of the ME

493 Capstone class. From these, a Product Design Specification (PDS) document was formed to identify key factors and this is summarized in the PDS table of Appendix A.

Compliance to competition rules, safety, reliability, cornering and ease of use were shown to be crucial to the success of the project. The team used the most important criteria from the PDS to grade various design choices in a decision matrix, shown in Appendix B. The results showed that the team should produce a leaning tricycle (steering independent of lean) with hub-centered wheels, a fairing, and a suspension device. The team was confident that these design attributes would fulfill the PDS requirements and provide a machine capable of performing well at the HPVC competition

[3] Evaluation of Final Design

A summary of the various product design specification targets and their evaluation results are presented in Table 1. Evaluation of the results was gathered during testing of the HPV during the 2011 HPVC in Bozeman MT. During the events scheduled, the team recorded its results and compared them to those set by the design team during the concept/design phase of the project. Due to an unfortunate accident during the speed trials, the team was unable to gather a true top speed for the HPV, but can safely say, it was less than 40 mph and maximum stable speed was also well below the goal of >40 mph.

Table 1. Summary of product design specification targets and there evaluation results gathered during the 2011 HPVC in Bozeman MT.

Metric	Target	Produced	Target Met?
Top Speed	**40 mph**	**N/A****	**No**
Acceleration	**0-15 mph, 5 sec**	**0-15 mph, 4 sec**	**Yes**
Turning Radius	**15 ft**	**7.5 ft**	**Yes**
Weight	**<40 lb**	**83 lb**	**No**
Braking Distance	**20 ft from 15 mph**	**12 ft from 15 mph**	**Yes**
Ground Clearance	**<7 inches**	**<5 inches**	**Yes**
Comfort	**Yes**	**Yes**	**Yes**
Packing	**4'x4'x8'**	**3.5'x3.8'x8'**	**Yes**
Maximum Stable Speed	**>40 mph**	**N/A****	**No**

****Indicate Product Design Specifications that were unable to be validated due to crash during HPVC.**

[4] Design Description

Previously, PSU HPV teams have made both recumbent three-wheelers and recumbent two-wheelers. Through testing of these older designs, it was discovered that the two wheelers were very unstable at low speeds. Low speeds and stops/starts are very important in the utility endurance event of the competition. Another key weakness of two wheel designs is the amount of practice necessary to use them. Since some of the race team was likely to see only a small amount of practice time, the more stable, three wheeled designs were deemed preferable, so only three-wheeled recumbent design concepts were generated. The team developed three possible frame designs as seen in Fig 1: delta lean-steer, tadpole lean-steer, and tadpole leaner with front suspension.

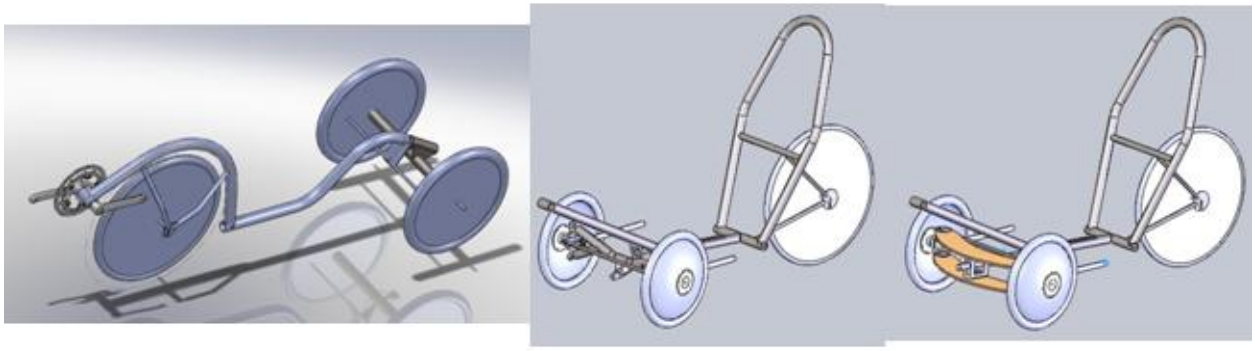

Figure 1. From left to right, the lean-steered delta trike, the rigid leaning tadpole and the leaning tadpole with front suspension.

The team chose the recumbent tadpole leaner with a front suspension design because it was likely to be more stable in smaller turning radii than a delta-style three-wheeler. The vehicle is rear-wheel drive and the front beam is a wood plank structure that acts as a suspension device.

The hub centered wheel was chosen to improve steering geometry. The distance from the contact patch of the tire to the point where the steering axis pierces the ground stays relatively constant with hub centered wheels, compared to designs where the steering axis is inboard of the wheel. This constant lever arm length means the transverse force on the wheel form cornering should then more predictably return the vehicle to straight, resulting in a more stable

ride. This style of wheel is useful mainly on multi-wheel HPVs where steering uses multiple tires. Between aluminum, fiberglass, Kevlar, and carbon fiber for the product material, carbon fiber proved to be superior because it is light, rigid, strong and could be easily formed into a dish shape.

The proposed steering design is shown in Fig. 2 significantly reduces the risk of injury by moving the hand position of the rider away from the ground, eliminating the risk of hand injury while leaning in a turn and hitting bumps. It also adds more power to the steering due to its forward and back movement compared to that of the side by side motion placed below the rider's seat.

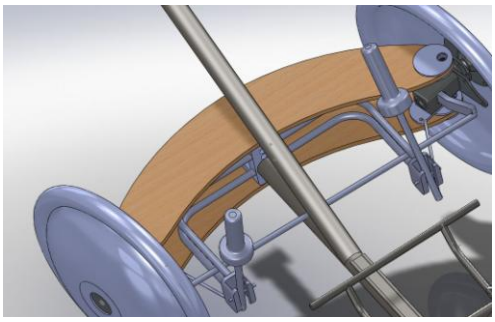

Figure 2. Two handle steering design with Ackerman.

However, due to money and weight restrictions set by the design team, the design finally settled on by the team was that of a side by side motion, placing the handlebars at the riders hips and coming out from the steering uprights. In Fig. 3 below, the final design built by the design team and used during the HPVC in Bozeman MT, shows the simplicity and ease of use for construction and handling while riding.

Figure 3. Final steering design for the 2011 HPV, with handlebars connected straight into steering uprights and set and hip level of the rider.

[5] Energy Storage Device vs. Fairing

The design team considered implementation of a regenerative energy storage device on board Mjölnir during the utility event even though the proposed system scored negatively as a lower-level component in the design matrix. The reason for this was that the decision matrix was constructed qualitatively from instinct and we felt a more detailed quantitative analysis was warranted to insure we did not miss an opportunity to include an extremely effective, innovative system.

Figure 4 shows the comparison of the two systems across the expected speed range. The 50%+ rider power output requirement increase was seen as adequate evidence that a fairing would outperform an energy storage device and was the correct system to include.

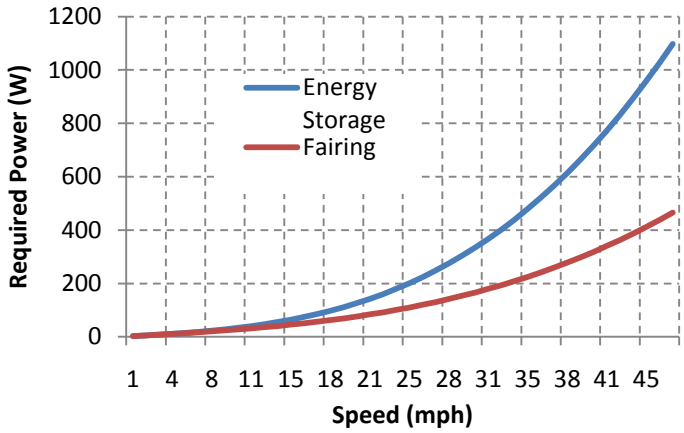

Figure 4. Power required to sustain Mjölnir's speed with either an energy storage device or aerodynamic device.

Additionally, it can be inferred that a higher maximum speed can be achieved with an aerodynamic device because the power output from a rider maxes out at around 350 W. A more detailed analysis of energy storage vs. fairing can be found in Appendix C.

The fairing design must meet the criteria of light weight, ease of use and a coefficient of drag less than 0.15. In recent years, teams have used everything from full fairing designs to simple nose cones. This year's preliminary design, shown in Fig. 5 is a partial fairing. It was chosen for its good aerodynamics yet ease of use. The rider does not need any assistance entering or exiting the vehicle, while still maintaining a drag coefficient of 0.1164. However, due to the time and money restrictions placed on the design team, a trimmed down version of the fairing had to be built. Shown in Fig. 6 below, the team built a simple nose cone to help reduce drag, and eliminate some of the weight associated with the preliminary design, however, no coefficient of drag was able to be calculated. More information on the preliminary fairing analysis and design can be located in Appendix D.

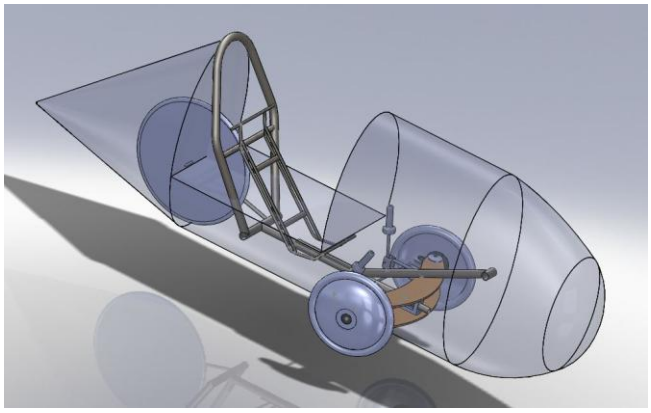

Figure 5. Preliminary fairing concepts

Figure 6. Fairing used in 2011 HPVC in Bozeman MT.

[6] Analysis and Testing

[6.1] Roll Over Protection System (RPS)

For the safety of its riders and the conformity to the HPVC rules, the 2011 Portland State University Human Powered Vehicle Team performed a deflection analysis on the vehicle's Roll-Over Protection System and validated the analysis with physical testing.

Analysis

The maximum deflection was to be evaluated against theoretical values using Finite Element Analysis (FEA). The roll bar must not exceed 2 inches of deflection from a 600lb load applied

downward and aft 12° from vertical at the top of the bar, or a 1.5 inch horizontal deflection from a 300lb horizontal load applied at shoulder height as stated in the 2011 HPVC rules and regulations. Any plastic deformation, deformation beyond the specified limits, or deformation that results in the frame coming in contact with the rider would be considered a product failure. Detailed analysis is presented in Appendix E.

Testing

The rollover protection system was tested as stated in the 2011 HPVC rules and regulation hand book. Top and side loading tests were performed in the machine shop at Portland State University in order to validate and inspect the safety of the vehicle. For the top loading test, weights in 25 lb increments where added and deflections where recorded. At 600 lbs the max deflection was 1.912 inches, giving the frame a factor of safety of 1.04 in the chance of complete 180° rollover. For the side loading test, the RPS was placed in a hydraulic press. Load was applied in 25 lb increments and deflection was measured. At 300 lbs, the max deflection was 0.3 inches, giving the frame a factor of safety of 5 for side impacts and 90° rollover. Refer to Appendix E for test figures and data.

[6.2] Hub Center Wheel

The carbon fiber wheels were required to have sufficient strength and stiffness without high weight to provide safety and high performance. Analysis and testing were conducted to optimize the thickness of the shell necessary to produce these qualities.

Analysis

FEA of the wheels was conducted with Abaqus CAE software. This analysis was conducted on shell geometry using the composite layup features in Abaqus and material data supplied by manufacturers of the carbon fiber and epoxy. The boundary condition applied to the model was x, y, and z translational restraint of the inner ring of the wheel simulating the rigid attachment of the wheel to the hub. The transverse loading was found to cause the highest

stresses in the part, and so was chosen to be the test case load. Fig. 7 shows the boundary conditions and transverse load applied to the FEA model.

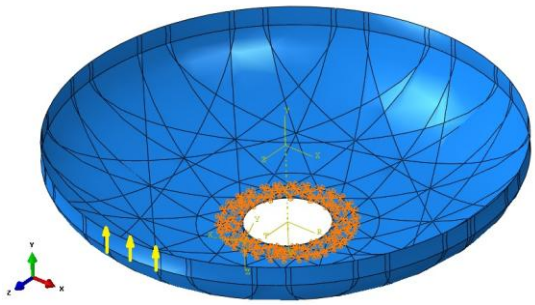

Figure 7. The FEA model of the carbon fiber wheel with the points near the center hole as the boundary conditions and the white arrows along the edge as the load. The partitioning seen is not a coarse mesh, but the divisions between the carbon strips of the layup.

This analysis produced a load/deflection curve, shown below in Fig. 8 that was validated by testing a sample wheel. Details of the analysis are given in Appendix G.

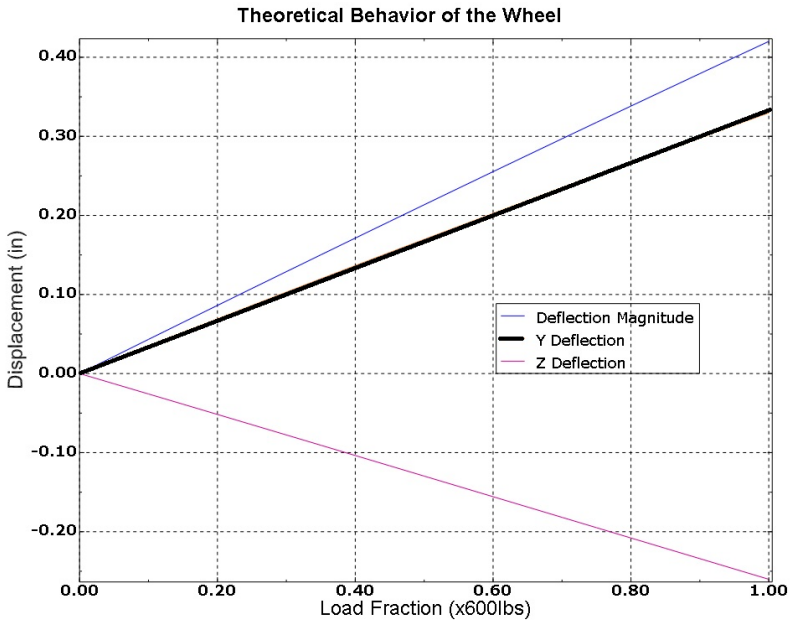

Figure8. Graph of the carbon fiber wheel displacement vs. load fraction

Testing

The strength and stiffness of the carbon wheels is extremely important to the performance and safety of the vehicle. Since the Abaqus FEA of these factors used composite layup and orthotropic materials, techniques previously unproven at PSU, it was decided to build a spare wheel and test it to validate the models. The test performed was a side load at the rim of the wheel to simulate the cornering forces that would cause the most likely mode of failure. Results from the test fell within 5% of the behavior predicted by the model, which allowed us to use the model to refine the wheel design for lighter weight. Slight delamination of the carbon shell from the aluminum rim was also encountered during testing at very high loads well in excess of those expected during operation. While it was decided this did not pose a significant safety hazard or threat to vehicle performance, it was cause to reexamine and improve the surface preparation technique used on the rim. Detailed test procedure and results are given in Appendix H.

[6.3] Suspension Arms

The design of the front suspension leaf springs was optimized using Abaqus CAE, but before this could begin, material properties for the material candidates were needed. Baltic Birch is a type of plywood used in many demanding applications such as skateboards and furniture. Its strength, low cost, light weight and attractive appearance made it the most appealing material to use. While some material properties were found through research, none were from reputable enough sources to use for design purposes so a four point bend test was performed to determine properties. This bending test was chosen since it creates a loading similar to that expected for the part, and can yield a flexure modulus (elastic modulus for bending) and rupture modulus (breaking strength for brittle materials in bending). Although wood is an orthotropic material, plywood in bending can be reasonably approximated as isotropic since alternating layers have perpendicular grain orientation and the bonding adhesive also contributes to the mechanical behavior. (Forest Products Laboratory, 1999) Results from this testing were average values for flexure modulus of 1.7Mpsi (11.9Gpa) and rupture modulus of 24.1ksi (166Mpa). When these properties were applied to Abaqus models of the proposed

design, behavior was very favorable and the Baltic Birch was selected over the alternate plan of a more rigid steel cross member. Appendix I contains the detailed procedure and results.

[7] Practicality

A major goal for the vehicle was a design that is practical for use as daily transportation in the design region of metropolitan Portland, OR, at least 300 days per year. The factors seen as most important to practicality are weather protection, street legality, stability, visibility, cargo capacity, comfort, and simplicity of maintenance. Portland has a mild climate with the exception of very frequent rain as can be seen in Table 2. This means that, based on a rideable temperature range of 41F (5C) to 95F (35C), riding is possible year-round except during the night hours in winter and hottest part of the day during summer heat waves. Rain protection, however, is very necessary. Commercially available wheel fenders were chosen as the most cost effective means to protect from water thrown by the tires, and the fairing was designed to provide enough coverage to protect from falling rain. Portland does not use salt on the roads, but since the frame is steel it was painted externally and treated internally with a sealant to prevent corrosion.

Table 2: Weather data for Portland, OR from NOAA (Local Climate Data from Portland Airport, 2009)

	Jan	Feb	Mar	Apr	May	Jun	Jul	Aug	Sep	Oct	Nov	Dec	Annual
Mean Max Temp (°C)	7.2	9.8	12.9	16.2	19.7	22.6	26.1	25.9	22.9	17.3	11.4	8.0	16.7
Mean Min Temp (°C)	1.8	3.1	4.6	6.4	9.2	11.8	13.9	13.9	11.9	8.7	5.2	2.9	7.8
Mean Rain (mm)	164	126	115	74	55	40	13	19	45	85	159	176	1069
Mean Rain Days (>0.25mm)	17	16	17	15	13	9	4	5	8	11	19	18	152
% of possible sunshine	29	38	48	52	57	56	69	66	62	44	28	23	48

The equipment legal requirements of ORS815.280 for cycling in Oregon relate to braking and lights for night riding. (Thomas, 2009) The braking requirement of a full stop from 10mph in 15

feet is less rigorous than the HPVC competition regulations, so this requirement is easily satisfied. Lights are required for riding in limited visibility conditions, and standard bicycle lights can easily more than meet these standards and are included. Additionally, a tail flag and bright colors are employed to increase visibility since recumbents have a low profile.

Various options were considered for carrying cargo, including racks, integrated bags, and compartments in the fairing. Based on the criteria of capacity, versatility and ease of access, a wide platform rear rack was selected. This rack is compatible with standard bicycle panniers, has a wide platform to ease carrying of large volume loads like grocery bags, and carries up to 45lbs.

A major reason that a tricycle configuration was chosen for the vehicle is the stability offered by three wheels. Full stops, low speed corners, novice riders, and awkward cargo loads are all common situations in commuting and errand running. Experimentation by the design team with standard bikes and previous PSU vehicles showed two-wheelers, especially recumbents, to have distinct disadvantages in these circumstances.

Specific goals for simplicity of maintenance were threefold; 1) all fasteners must be metric to match the metric standard on bicycle components, 2) a normal bicycle shop should be able to perform all regular maintenance, and 3) all consumable parts should be readily available and non-proprietary. Fasteners and consumable parts such as bearings and drive train components were specified accordingly, and local mechanics were consulted to insure maintenance tasks were not beyond the reach of their skills or tools. In addition, an internally geared hub was specified in the drive train to reduce the number of scheduled maintenance tasks and consumable parts.

[8] Safety

Rider safety is paramount, and its consideration must be accounted for in the design. Risks that are involved in the operation of the machine had to be identified, evaluated, and finally

mitigated to assure the chance for rider or possible pedestrian/spectator injury is as close to zero as possible.

[8.1] Rollover

The potential of machine rollover is a hazard and a risk that must evaluated and mitigated. Shown below in Fig. 9 is the velocity at which rollover will occur plotted against the corner radius. This was done by considering the counteracting moments of rider/machine weight and radial force about the contact patch of the tire. This analysis gave the team a concrete idea of the real possibilities for rollover in the competition and details are shown in Appendix J. To mitigate this risk, the HPV's frame will lean in and out of corners. As the frame leans this decreases the height of the center of gravity, which shortens the radial force moment arm, ultimately increasing the rollover velocity. The leaning design lowers the possibility of rollover and makes the HPV a safer machine.

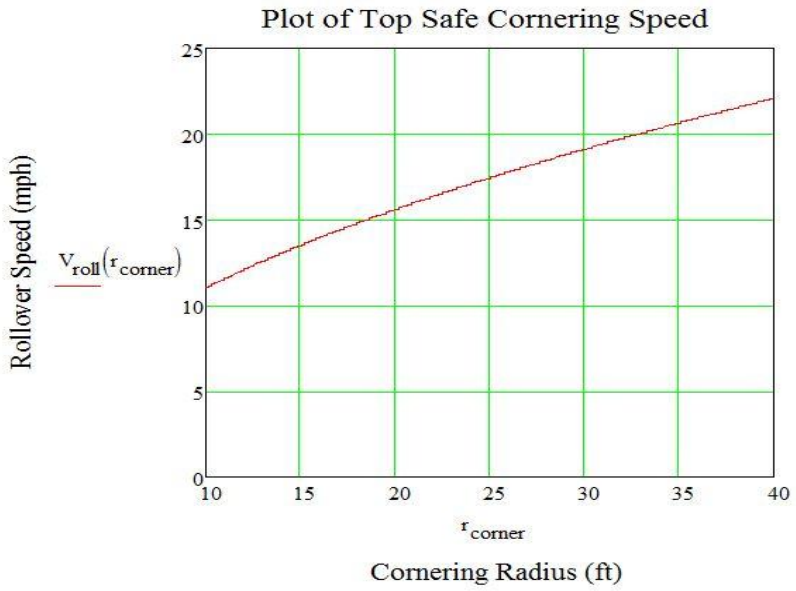

Figure 9. The speed at which rollover will occur versus the corner radius of the vehicle.

[8.2] Visibility

Visibility can be limited with the use of a full fairing. The team decided to mitigate this safety concern with an open cockpit style fairing. In doing so, the team's peripheral vision is less obstructed. By expanding the field of vision, the rider has a better feel for his/her surroundings when encountering obstacles and other riders. A rear view mirror is also be used to enhance the rider's visibility. By expanding the rear field of vision the team can reduce potential for rider collision and possible rider or pedestrian/spectator injury.

[8.3] Steering

A concern of the team was steering control location and how the hands of the rider could encounter hazards while leaning the HPV during cornering. To keep the rider's hands free from contacting the ground or any other hazard, the steering controls are located just in front of the rider's chest. This completely eliminates the chance of the rider injuring his/her hands while steering and also gives an intuitive, ergonomic hand position.

[9] Failure Analysis

The team was confident in our ability to do well in the competition that Mjölnir was built for, but we suffered a debilitating crash during the first event, a top speed test with a 500m run-up to a 100m time trap. The driver lost control and hit a hay bale at approximately 20mph, completely shearing off the right side of the front suspension as seen in Fig. 10. This was an extreme disappointment since we did not have adequate spare parts to make repairs in time to continue racing that day, but it did provide the unique opportunity to analyze a failure.

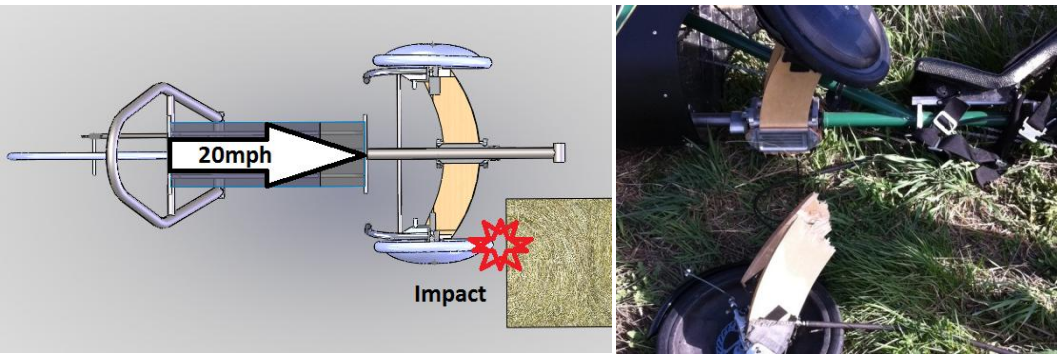

Figure 10. The right front wheel took the full impact of the crash in the sprint event and the suspension arms broke at their bases as a result.

The cause of the crash was perceived to be a combination of vehicle instability and a wind gust. The wind was very intense, with gusts up to ~50mph, and this environmental factor is obviously beyond our control, but vehicle stability was a major design goal so this deserved further investigation. Several possible contributing factors and possible solutions were identified:

- Narrow track: The vehicle's narrow track width was specified to reduce frontal area with the intention that leaning into a turn would move the center of mass and prevent tipping. When the leaning mechanism was locked out since it was ineffective the track width was then too narrow to effectively prevent tipping. A wider track width is recommended.
- Toe-in: A slight toe-in configuration of the front wheels is used to provide straight-line stability for many vehicles, human powered and otherwise. Too much and an oscillation between one tire getting more traction than the other can occur. This may have caused the shimmy the driver noticed immediately before the crash. A better system for accurately measuring and adjusting toe-in should be implemented.
- Direct steering: The steering mechanism of a handlebar directly connected to the upright provided a side-to-side steering input motion which was difficult to keep centered at high speeds. A steering damper or linkage actuated steering are possible solutions.

The suspension arms were not designed to take this kind of impact, and insufficient material data was available for the wood to determine if failure in this mode was to be expected. What

was possible was to model previous years' PSU HPVs with FEA software to determine if this is an impact that most should survive. Results of these analyses showed that not only did all of the vehicles fail in these conditions, but all did so in a way that rendered the majority of the frame unusable. The fact that the only components to fail were the suspension arms and the drag link connecting rod shows that the design has a robustness that was not even intended. Availability of adequate spares, however, is advisable if this design is to be used in the future.

Another positive result of the crash is that the driver was completely unharmed. This was a good validation of safety features of the vehicle such as the restraint system.

[10] Aesthetics

To enhance the overall impression of the vehicle, a variety of visually appealing materials and techniques were employed. The vehicle's performance was of paramount importance, but appearance of the vehicle is important to customers of such a high-end device as well.

[10.1] Surface Finishing

The frame was painted with enamel to protect against corrosion. To protect the inside of the frame, ⅛" drain holes were drilled and a rust inhibitor (Loctite Extend Rust™) used to coat the inside walls. Painting the aerodynamic fairing provided the same results as the frame: protection from the elements and concealment of imperfections in the material that result from casting. Wooden components are coated in a clear epoxy to protect from water absorption and add a desirable gloss to the components.

[10.2] Component Aesthetics

Sustainability of materials was a significant factor in deciding to use a wooden suspension device. This material also provides good contrast with the other components invoking a visual

and ethical stimulation in the customer.

With the fairing in place, the additional exposed components are the front wheels. The outboard sides of the carbon fiber composite wheels are to be polished to display the desired aesthetic of carbon fiber weave.

[11] Conclusions and Recommendations

Although the prototype suffered a front end collision, the 2011 PSU HPV team won third place in design. The mishap was an opportunity for the team to reflect on the causes of failure. The information recovered from the incident will help following HPV designs to avoid the same mistakes the team encountered. Had the prototype not broken down, its design flaws would have remained hidden, and mistakes ignored. Failure is a part of success as long as its causes are revised and treated.

In engineering, there is a constant need for improvements as there is a never ending list of flaws. These flaws, with the correct processes, can and should be predicted and dealt with before catastrophic failure. Mitigating the cause of failure of the suspension, found to be instability of vehicle coupled with unexpected material properties, could have been accomplished with more testing.

Unknown physical phenomenon (such as the leaning mechanism) would be best explored by modeling. A physical scale model would have proven the instability of this system, as it was used, and pointed the team toward a more practical solution earlier in the design process. Dynamic modeling software would have been useful, but only as a preliminary step before physical testing.

A thorough risk analysis could have uncovered the possibility of failure that the wooden planks experienced in the particular mode of failure that occurred. Due to the variation of material properties available for the wood composite chosen, multiple questions should have been

raised as to the practicality of its use.

The team learned valuable lessons through the problems encountered in the testing of the prototype: 1) Choose a simple, practical solution to the problem, 2) Try to uncover design flaws and problems before they show up by modeling the solution analytically and physically, 3) eliminate the problem of “5 engineers with one pencil” and consider all ideas an thoughts valid and prove them significant or not with appropriate analysis, and 4) predict, test, verify, and repeat.

[12] Appendices

[12.1] Appendix A: Product Design Specifications Table

Product Design Specifications table generated by 2011 HPV design team to validate decisions made in areas deemed most important. PDS was used throughout the design and construction process.

Priority	***Requirement***	***Customer***	***Metric***	***Target***	***Target Basis***	***Verification***
Performance						
3	Top Speed	ASME/Self	Mph	40 mph	Industry Expert	Testing
3	Acceleration	ASME/Self	Mph/s	0-15 mph, 5sec	Industry Expert	Testing
3	Maneuverability	ASME/Self	Small turn radius	15 ft	Competition Rules	Testing
2	Weight	ASME/Self	Lbs	<40 lbs	Benchmarking	Testing
1	Fairing (Cross Sectional Area)	ASME/Self	Ft^2	<4 ft^2	Benchmarking	Comp. Fluid Dynamics
1	Fairing (Coef. Of Drag)	ASME/Self	-	<.12	Benchmarking	Comp. Fluid Dynamics
1	Braking Distance	ASME	20ft from 15mph	<20 ft	Competition Rules	Testing
2	Ground Clearance	ASME/Self	Inches	7 inch	Industry Expert	Testing
3	Maximum Stable Speed	Self	Mph	>40 mph	Industry Expert	Testing
Practicality						
2	Comfort	ASME/Self	Yes/no	Yes	Benchmarking	Testing
1	Packing	ASME/Self	Height x Width x Depth	4'x4'x8'	Transport Vehicle	Design Measurements
3	Ease of Use	ASME/Self	Yes/no	Yes	Benchmarking	Testing
Maintenance						
2	Reliability	Self	Service Life	Yes	Benchmarking	Competition Score
2	Accessibility to Components	Maintenance	Personnel required	2	Benchmarking	Manufacturing
2	Availability of Parts	Maintenance	Part lead time	2-3 days	Benchmarking	Manufacturing

Priority	*Requirement*	*Customer*	*Metric*	*Target*	*Target Basis*	*Verification*
Maintenance (cont'd)						
2	Uses Standard Tools	Maintenance	Yes/no	Yes	Benchmarking	Manufacturing
2	Maintenance Interval	Maintenance	Miles	500	Benchmarking	Maintenance
2	Maintenance Time	Maintenance	Minutes	90	Benchmarking	Maintenance
Materials						
1	Aesthetics	ASME/Self	Visual Appeal	Stunning	Market Analysis	Competition Score
Documentation						
3	Final Report	ASME/Self	Deadline Date	May 13th	Competition Rules	Course Evaluation /Competition Score
Safety						
3	Visibility (Horizontal)	ASME	Degrees	180	Competition Rules	Testing
3	Visibility (Vertical)	Self	Degrees	>45	Benchmarking	Testing
3	Rollover Protection System Top Load	ASME	Lbs	600 lbs	Competition Rules	Testing
3	Rollover Protection System Side Load	ASME	Lbs	300 lbs	Competition Rules	Testing
2	Rider Restraint	ASME	Pass/Fail	Pass	Competition Rules	Testing
3	Frame Safety	Self	Factor of Safety	F.S.>1.5	Benchmarking	Testing
Budget						
3	Materials/ Fabrication	ASME/SALP	US Dollars	<$3500	Funding Cap (SALP)	Final Documentation
3	Travel	ASME/SALP	US Dollars	<$2000	Funding Cap (SALP)	Final Documentation

Legend: High = 3 Medium = 2 Low = 1

[12.2] Appendix B: Top Level Design Decision Matrix

Decision matrix generated by the design team in order to validate the decisions need to produce the best possible solution based on design criteria most important to the design team. Design options are based on a numerical scale with 1 being the lowest and 5 being the highest.

	Rules Compliance	Weight	Reliability	Looks	Top speed	Cornering	Comfort	Safety	Ease of use	$	Manufacturability	Maintenance	Simplicity	**Totals**
Importance	5	3	4	2	3	5	2	5	4	2	3	1	3	
2 wheel	3	5	5	3	5	3	4	3	2	5	3	5	5	156
3 wheel rigid	3	4	4	4	4	4	3	4	3	4	3	4	4	154
3 wheel indep. steer	**3**	**3**	**4**	**5**	**4**	**5**	**5**	**5**	**4**	**4**	**3**	**3**	**4**	**170**
3 wheel integrated	3	3	3	5	4	5	5	5	5	4	3	3	3	167
Regenerative Assist	-1	-1	-	1	1	-	1	-	2	-1	-1	-1	-1	-2
Hub Center Wheel	**-**	**1**	**-**	**1**	**-**	**1**	**-**	**-**	**-**	**1**	**-1**	**-**	**-1**	**6**
Front Wheel Drive	-	-2	-1	1	-1	-1	-	-	-	1	-1	-2	-2	-27
Suspension	**-**	**-1**	**-**	**1**	**-**	**-**	**2**	**1**	**1**	**1**	**-1**	**-1**	**-1**	**3**
Fairing	**1**	**-1**	**-1**	**1**	**2**	**-**	**1**	**1**	**-1**	**2**	**-1**	**-**	**-1**	**7**

[12.3] Appendix C: Electrical Assist vs. Fairing Analysis

Energy Consumption Analysis: The Design team was faced with a decision, due to personnel and budget, between implementing an energy storage device (ESD) or an aerodynamic device (fairing) to reduce the amount of energy spent by the rider. The faring is required by ASME HPVC rules but can be eliminated for a deduction in design points. The team decided to compute the amount of energy spent with each device to choose the most efficient configuration for the vehicle.

Given: A comparison between fairing and ESD is to be performed to find which design will require the least power to operate. The governing equation 1A for power is given by Wilson as:

$$\mathbf{P_{required}} = \mathbf{K_1 mgV} + \frac{\mathbf{1}}{\mathbf{2}}\boldsymbol{\rho}\mathbf{AC_D V^3} \quad (1C)$$

And the required energy due to drive train efficiency is given by Cengel as equation 2A:

$$\mathbf{E_{required}} = \frac{(\mathbf{P_{required}} * \mathbf{t})}{\boldsymbol{\eta}} \quad (2C)$$

where *K1* = rolling resistance coefficient for typical bicycle, *m* = mass of vehicle + rider + component (kg), *g* = gravity (m/s^2), *V* = vehicle speed (m/s), ρ = air density @ 4800 ft elevation (kg/m^3), *A* = effective cross-sectional area of vehicle (m^2), C_D = vehicle coefficient of drag, *t* = time (hr), and η=drive train efficiency (%).

Find: Energy consumed by each design over length of competition.

Assumptions:

- Average speed over competition is 20 mph (9 m/s)
- Weight of both designs are comparable
- 90% drive train efficiency
- Neglect drag of electric drive motor
- Energy storage device remains on vehicle for entire competition

- Entire competition will take approximately 5.1 hours and utility event will take 2.5 hours
- Partial fairing (nose cone) has an assumed C_D = 0.3 (Models indicate lower)

Solution:

Results were tabulated using Microsoft® Excel with sample calculations for each design shown below:

$$P_{required\ (ESD)} = (0.0053)(104\ kg)\left(9.81\ \frac{m}{s^2}\right)\left(9\frac{m}{s}\right) + \frac{1}{2}\left(0.7595\ \frac{kg}{m^3}\right)(0.5\ m^2)(0.7)\left(9\frac{m}{s}\right)^3 = 145.56\ Watts$$

$$P_{required\ (fairing)} = (0.0053)(104\ kg)\left(9.81\ \frac{m}{s^2}\right)\left(9\frac{m}{s}\right) + \frac{1}{2}\left(0.7595\ \frac{kg}{m^3}\right)(0.6\ m^2)(0.3)\left(9\frac{m}{s}\right)^3 = 98.50\ Watts$$

For the utility event:

$$E_{required(ESD)} = \frac{(145.56\ W)(2.5\ hr)}{0.90} = 404\ W \cdot hr$$

$$E_{required(fairing)} = \frac{(98.50\ W)(2.5\ hr)}{0.90} = 274\ W \cdot hr$$

For entire competition:

$$E_{required(ESD)} = \frac{(145.56\ W)(5.1\ hr)}{0.90} = 825\ W \cdot hr$$

$$E_{required(fairing)} = \frac{(98.50\ W)(5.1\ hr)}{0.90} = 558\ W \cdot hr$$

Conclusion: The fairing configuration requires the least amount of power to operate and may be used over the entire competition as opposed to the ESD configuration's ability to be used for only the utility endurance event. For these reasons, the team chose to employ the fairing.

[12.4] Appendix D: Fairing Computational Fluid Dynamics

Comsol Multiphysics CFD software package was used to generate flow fields around fairing models to determine coefficient of drag, C_d, of fluid on fairing for design selection.

Restrictions of fairing design

- Width of roll bar (23.5 in)
- Height of toe-box (lowest point of heel to highest point of toe in a rider's pedaling motion) must be a minimum of 27 inches
- Clearance from ground (2.5 in)
- Height of roll bar from ground (42 in)
- Length of 10 ft. due to transportation restrictions

Assumptions:

ρ = 1.2 kg/m2 (density of air)

V_{max} = 15 m/s

Area = 694 in^2 (frontal area)

Based on the restrictions above, a fairing model was generated and placed in a fluid domain. The selection of 10m x 5m x 5m was used to allow proper development of flow without sidewall interactions based on the assumption that far field effects of fluid flowing around object are assumed to be zero at a magnitude of 10 radii away. Inlet velocity of 15 m/s and outlet boundary condition set to zero pressure (Pa) where chosen. No-slip boundary condition was selected for the surface of the fairing and moving wall boundary conditions on all remaining boundaries. The moving wall condition was selected to be 15 m/s to simulate the rider traveling in still air at 15 m/s down the course. Stationary solver was used due to computational time restriction. Since drag is not time dependent, the stationary solver was valid. Shown below in Fig. D-1 is the CFD of the model.

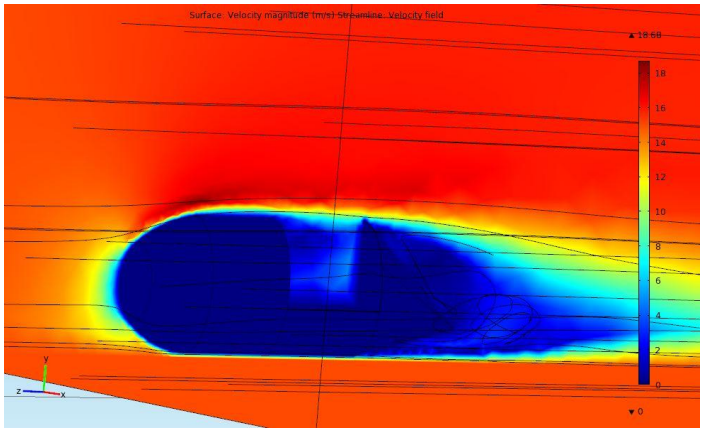

Figure D- 1. Velocity field around the model.

Stagnation points at the apex of the nose, as well as velocities as low as 2 m/s behind the tail were calculated, and matches flow theory. Turbulence can be seen by the streamlines at the trailing end of the fairing indicating to the design team that further refinements to the design need to be completed in order the reduce the pressure drag on the tail of the vehicle. Fig. D-2 shows the mesh element size used in the CFD model.

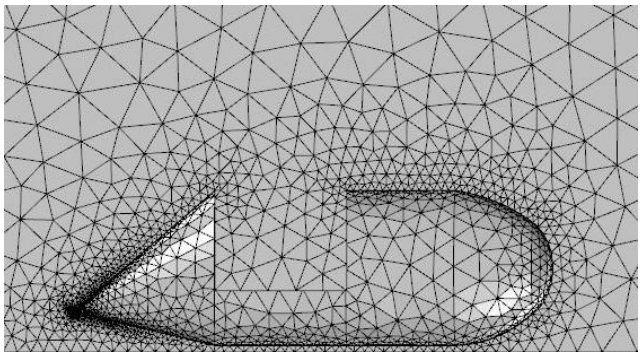

Figure D- 2. Velocity profile of fairing traveling at a velocity of 15 m/s. Moving wall boundary conditions are used to simulate rider traveling at 15 m/s in still air. Streamlines show fluid path around fairing.

Determining the coefficient of drag

To determine the coefficient of drag on the fairing, we integrated force over the front area of the fairing. This value becomes the drag force, F_d, in Eqn. 1D (Incropera, 2007).

$$\boldsymbol{F_d = \frac{C_d v^2 \rho A}{2}} \qquad \text{(1D)}$$

With F_d given by CFD model and all other constants known, we then found our coefficient of drag, C_d on our fairing. Theoretical values of C_d for streamline bodies are given as 0.06. Our design model showed a value of 0.1164 for C_d. All wheel cutouts and imperfections were neglected for calculation purposes. Figure D-3 shows the very small changes in C_d as the velocity of the vehicle increases.

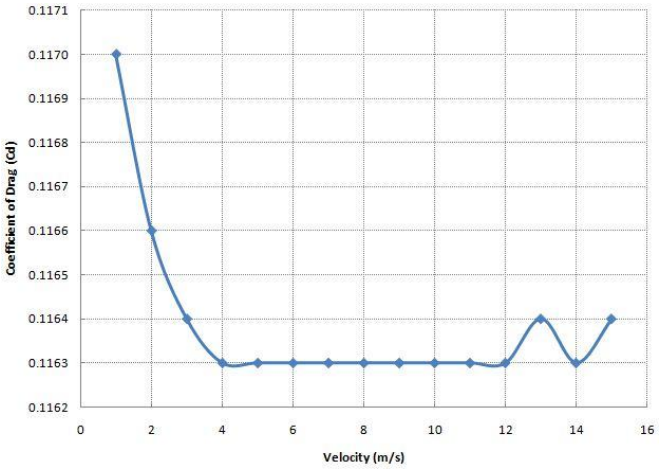

Figure D-3. Coefficient of Drag vs. Velocity of CFD model of fairing design.

[12.5] Appendix E: Analysis of Roll Over Protection System

To analyze the strength and rigidity of the roll bar design, a model of the frame was constructed in Abaqus finite element software from 3D, quadratic formulation, beam (B32) elements and subjected to a simulation of the tests specified by the competition rules. Boundary conditions imposed were x,y,z translational restraint where the seat stays meet the seat brace, and x,y translational restraint where the seat will be mounted to the main tube. These reflect the points that would be active in restraining the rider to the vehicle in a rollover. The first load applied was a 600lb concentrated force at the top of the roll bar, 12° from vertical, downward and toward the rear of the vehicle as specified by the competition rules. The second was a 300lb concentrated force applied horizontally at the widest point of the roll bar. These loads were applied separately, but Figure E-1 shows these conditions together for simplicity.

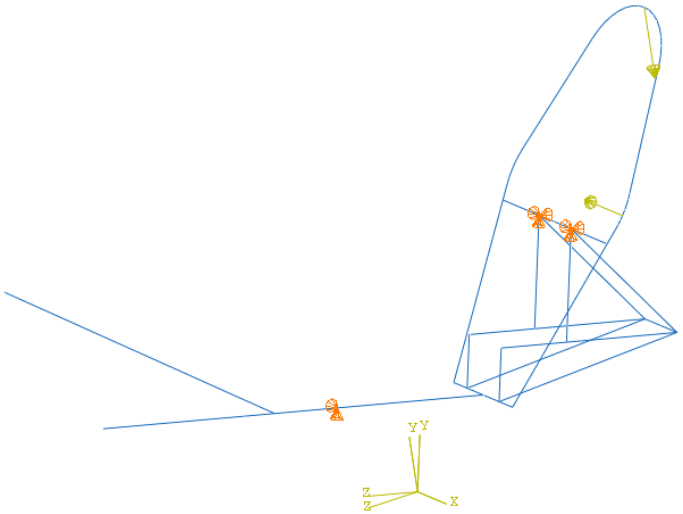

Figure E-1: Boundary conditions and loads. The two coordinate systems (CS) are the part global CS and the load CS that was rotated by 12° to orient the top load at the correct angle. The extra frame members not seen in further representations are geometric aids and were not meshed for analysis.

Figure E-2 shows the deformation of the frame, while figure E-3 shows stress at the point of maximum stress.

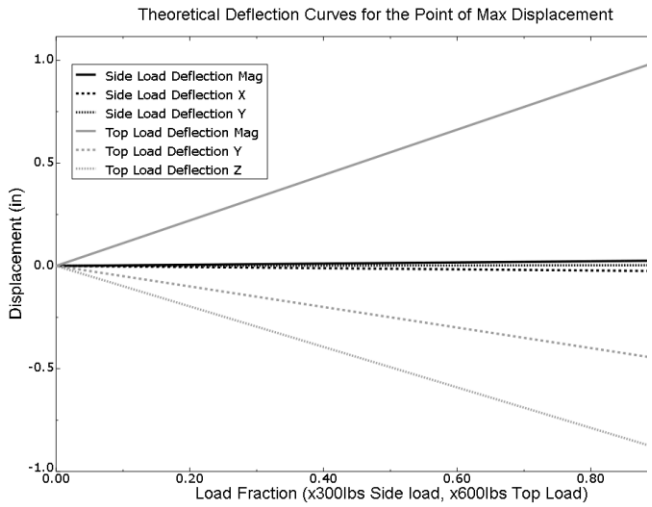

Figure E-2: Deflection behaviors. Of note is that the top load produces deflections an order of magnitude greater than the side load.

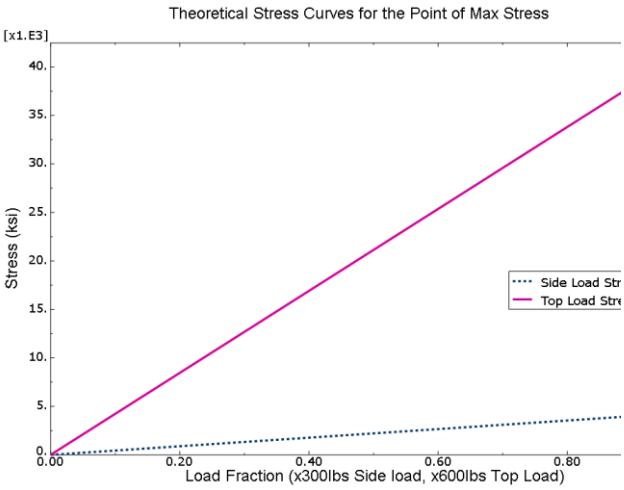

Figure E-3: Stress behaviors. Again, the side load produces much smaller results.

Deformed properties from the top load were found to be: maximum stress of 42.3ksi, maximum deflection of 1.104"magnitude, -.985" Z (rearward), -.500" Y (downward). From the top load, these properties were: maximum stress of 4.4ksi, maximum deflection of 0.028" almost exclusively in the -Y direction. These maximum stresses are well below the 60ksi yield stress of the material (FS = 1.41). The shape during loading and locations of the maximum deflections and stresses are depicted in Figure E-4.

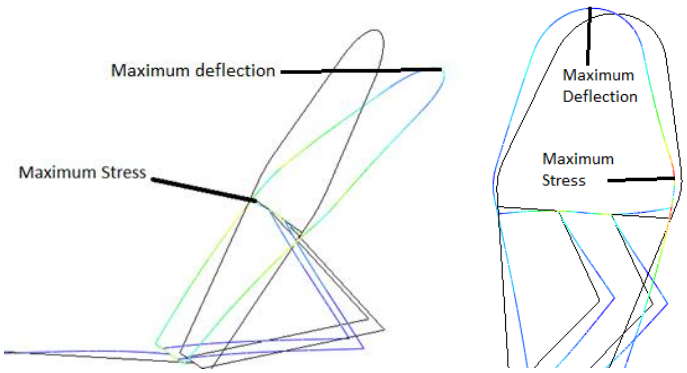

Figure E-4: Deformed shape (exaggerated) and location of maximum stress for the \top loading (left) and side loading (right)

[12.6] Appendix F: Rollover Protection System (RPS) Testing

The RPS was tested as stated by the 2011 HPVC rules and regulation hand book. Top and side loading tests were performed in the machine shop at Portland State University in order to validate and inspect the safety of the vehicle. Table F1 below shows the data gathered from the two experiments.

Table F1. Data collected during RPS testing.

	Top Loading	Side Loading
Load (lbs)	600	300
Maximum Deflection (in)	1.912	0.3
Maximum Deflection allowable (in)	2	1.5
Factor of Safety	1.04	5

Finite Elemental Analysis was performed on the model of the RPS and compared against the data gathered from the testing done on the RPS by the design team. Figure F-1 shows the RPS deflection as a function of load for both experimental and theoretical values.

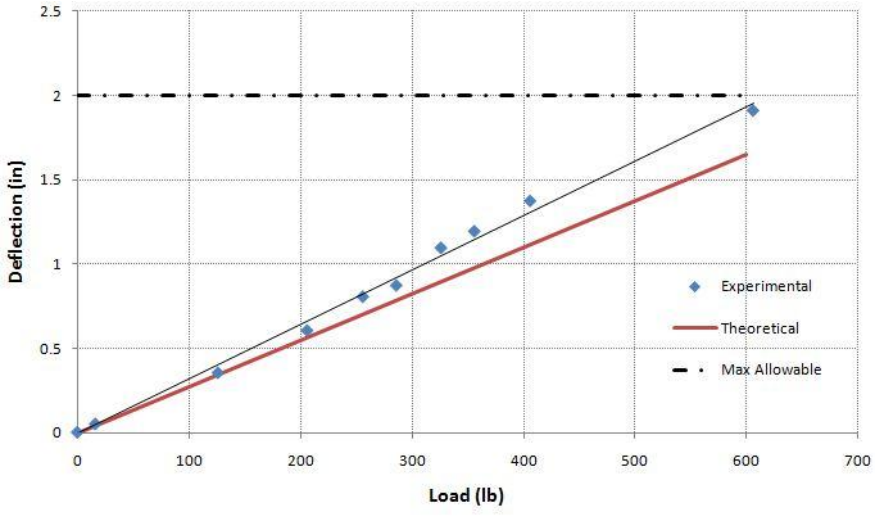

Figure F-1. Deflection vs. Load of the RPS during top loading with a maximum deflection of 2 inches allowable for a load of 600 lbs

Figure F-2 and F-3 show the boundary conditions used in the FEA model and experimental RPS test.

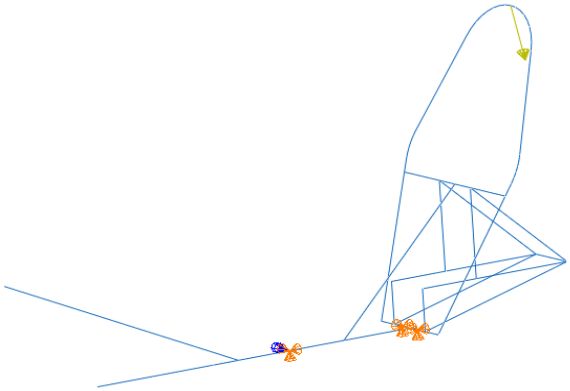

Figure F-2. Boundary conditions of frame in FEA model. Top loading, 12 deg aft is shown by yellow arrow. Fixture locations are represented by orange symbols.

Figure F-3. Boundary conditions of frame RPS testing setup. Orange symbols represent fixture locations. Yellow arrow represents applied load.

Using the FEA model mentioned above, the design team looked at max stress concentrations on the frame under the same loading conditions as the top loading scenario. A maximum von Mises stress of 38.4 ksi was found at the shoulder height of the RPS. Figure F-4 below shows the location of the stresses in the RPS in the FEA model.

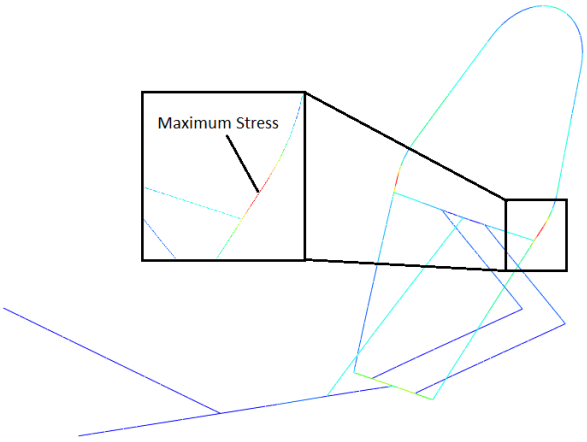

Figure F-4. Maximum von Mises stress of 38.4 ksi located at the shoulder height of the RPS in the FEA model

[12.7] Appendix G: Carbon Fiber Wheel Analysis

To insure the safety of the carbon fiber hub centered wheels and optimize the design for stiffness and weight, they were analyzed with Abaqus FEA software.

Given:

The part to be modeled and tested is a heavily dished carbon fiber shell wheel with an aluminum rim. It is to be made of a layup of unidirectional carbon fiber strips onto the rim in a patterned epoxy resin composite. Material properties have been found from supplier documentation to be those shown in Table G-1.

Table G-1. Material data as supplied

Material	E,x (GPa)	E,y (GPa)	ν	G,xy (GPa)	G,xz (GPa)	G,yz (GPa)
Carbon Layup	135	10	.3	5	5	5
Aluminum	70	NA	.33	NA	NA	NA
Bulker Foam	5	NA	.4	NA	NA	NA

Geometry is to be that imported from the 3D Solidworks models used for part form design. Load is a 600lb load transverse to the wheel plane at the rim to simulate double the maximum expected reaction force from the road in hard cornering.

Find:

a) Maximum stress and its location, as well as a factor of safety
b) Maximum deflection and its location

A model was created with Abaqus CAE software from 8-node, doubly curved, quadratic formulation shell (S8R) elements. Boundary conditions imposed were x,y,z translational restraint of the locations of the surface to be restrained in testing. Load applied was a 600lb shell edge load along a 45mm section of the rim edge, parallel to the axis of the wheel.

Results from this model show a maximum deflection in the load application region of 7.05mm as shown by Fig. G-1.

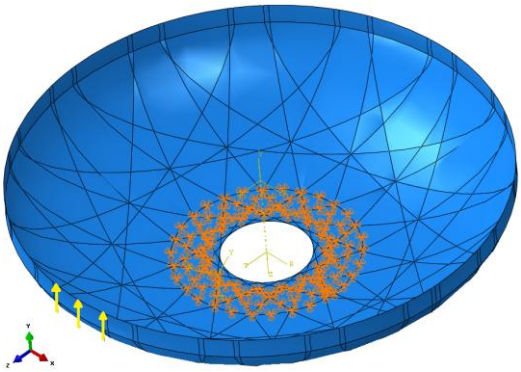

Figure G-1. Boundary conditions and load.

The part was partitioned into regions, which are visible in Fig. D-6, and is based on the edges of the unidirectional carbon strips to be laid on the part. The section of the shell was created using the Composite Layup feature, which enabled the placement and orientation of the strips of carbon to be described, rather than specifying the section and fiber direction combination of each individual region.

A Medial axis free mesh of 5570 elements, 16,730 nodes was used, a segment of which is shown in Fig. G-7.

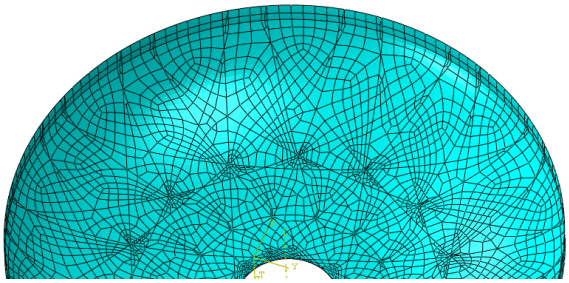

Figure D-7. Representative segment of the mesh used. The areas of high concentration of small elements were inevitable since small element regions were created by the partition line intersections.

Maximum stresses found at the discontinuities where elements are “pinched” as shown in Fig. G-2 was disregarded. Reliable, even field maximum stresses were found to be around 260MPa in locations shown in Fig. G-2

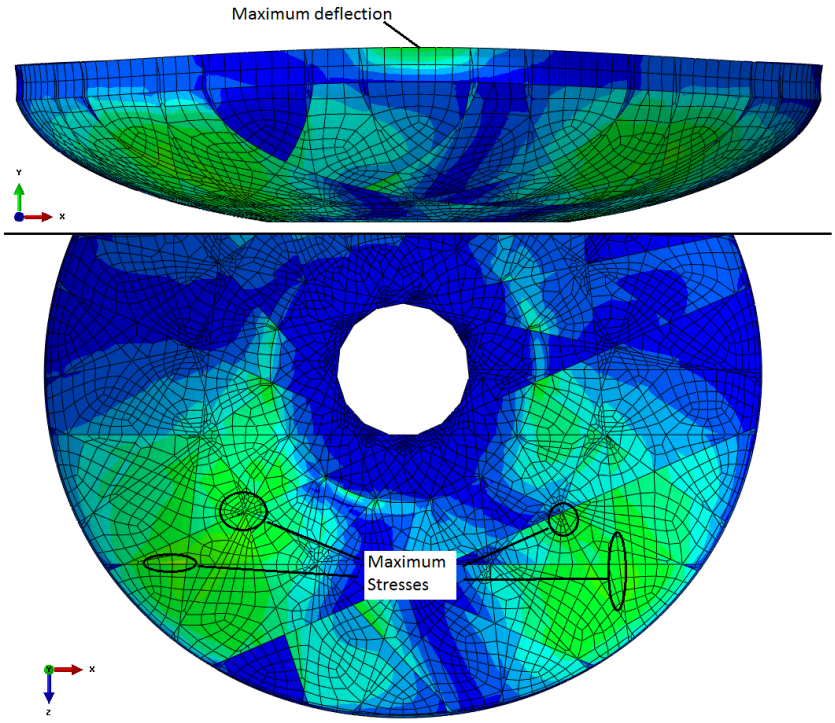

Figure G-2. Areas of maximum stress and deflection. Circled areas of maximum stress indicate where the actual peak stresses occurred, but large parts of the lighter areas in the figure showed stresses within 20% of the maximums.

The analysis also yielded the deflection/load plot of Fig. G-3.

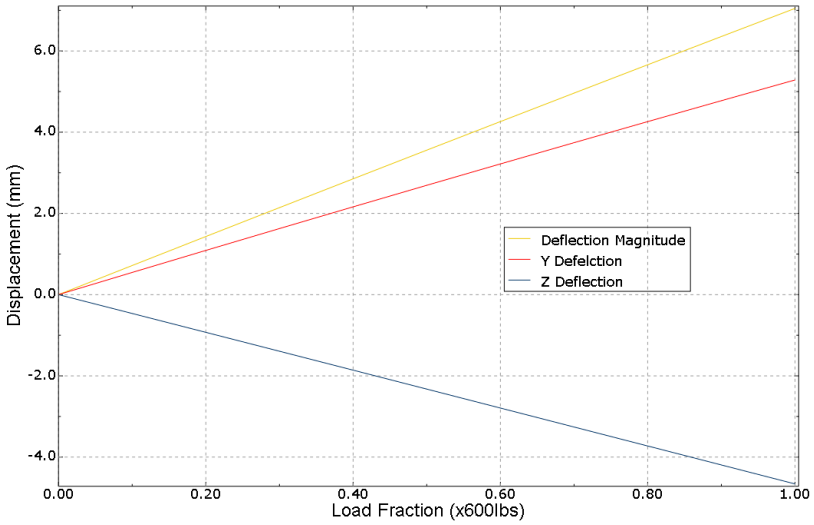

Figure G-3. The load curve in magnitude and components.

Using a typical tensile strength of 2,700MPa as provided by the manufacturer, the maximum stresses give a factor of safety of over 10. This is a very large safety factor, especially since the load applied is already twice the expected load, but the decision was made to proceed with this design since a decrease of rigidity would be detrimental. Once physical testing was completed to validate the model, it was used to optimize the design for reduced weight.

[12.8] Appendix H: Carbon Fiber Wheel Testing and Refinement

The carbon fiber dish wheels that are employed in Mjölnir must be rigid and strong enough to minimize deflection and the chance of failure under loading caused by cornering and braking. To verify the Abaqus CAE models used to optimize the design for weight, stiffness and strength, a test was performed to compare the deflection under load to that predicted by the models. Maximum stresses in the models were found to occur from transverse loads caused by cornering, so this condition was selected for the test. To match the boundary conditions and load applied in the model, the wheel was attached to a fixture in a compressive test load frame as shown in Fig. H-1.

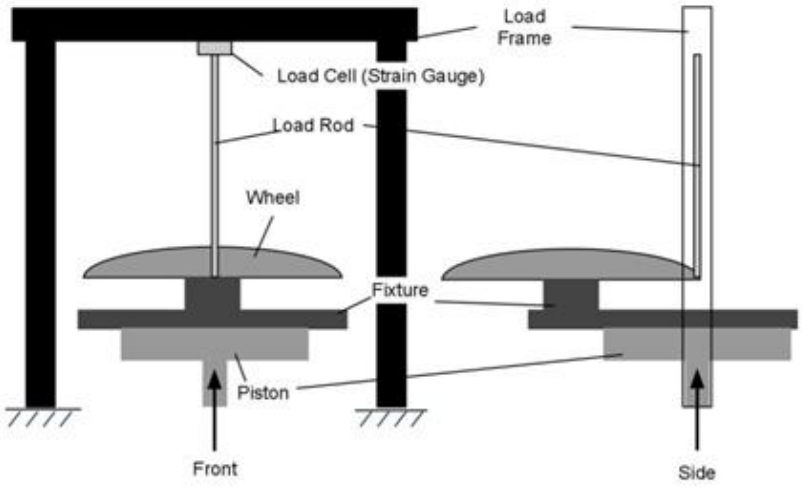

Figure H-1. The fixture of 1in steel plate is clamped to the load piston; the load rod is threaded into the load cell and rests against the rim of the wheel to apply the load force as the piston moves up.

A worst case scenario of the entire cornering load from a 225lb (102kg) rider being applied to one wheel in a 15ft (4.57m) radius turn at 15mph (24kph) was chosen resulting in a 225lb (1003N) transverse load. This maximum load was increased to 600lbs (2670N) for the test to explore behavior in overloading. Fig. H-2 shows that the wheel performed according to the model, and less than a 6% error was measured for both maximum deflection and load/deflection ratio.

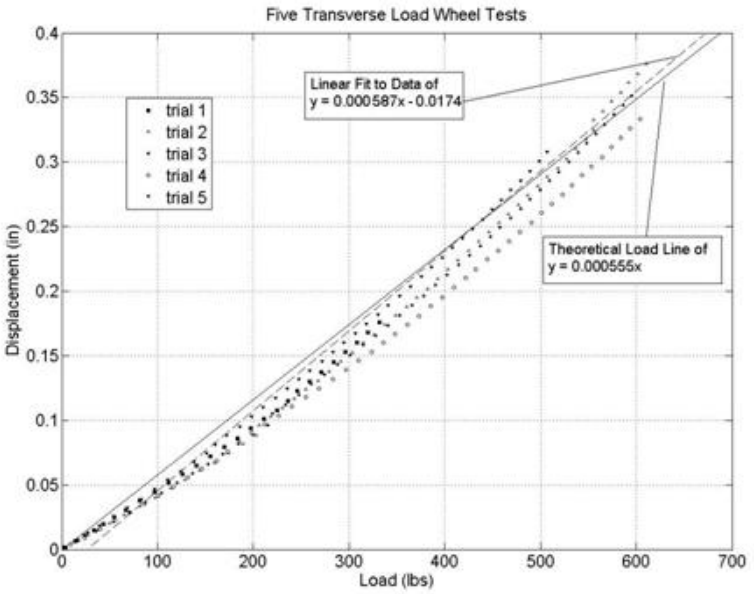

Figure H-2. Though the part behavior is less linear than the model, the strength of the carbon wheels has been proven and the linear behavior of the model is within the error of the experiment.

The average measured maximum deflection of 0.357 in. at max load of 600lbs has an error of 5.18% from the modeled maximum deflection of 0.333 inches. The deflection rate for each experimental trial was obtained directly from the slope of the linear curve fit equation similar to that in Figure G-2. Linear regressions of each trial were performed, yielding a mean deflection rate of 5.87×10^{-4} in/lb (3.35×10^{-6} m/N) with a standard deviation of 4.37×10^{-4} in/lb (2.50×10^{-6} m/N). This gives a 95% confidence interval for the deflection rate being between 4.62×10^{-4} in/lb (2.64×10^{-6} m/N) and 7.04×10^{-4} in/lb (4.02×10^{-6} m/N.

Confident that the model was an accurate tool, it was then used to refine the layup pattern of the wheels to reduce their weight by 20%.

[12.9] Appendix I: Baltic Birch Material Testing

The team needed material data, specifically a flexure modulus and rupture modulus, for Baltic Birch plywood in order to determine if this was an appropriate material for the front suspension so a four point bend test to failure was performed on four test samples. A four point bend test is loading of a beam as shown in Figure H-1, so that the center section has a constant moment between the downward loads.

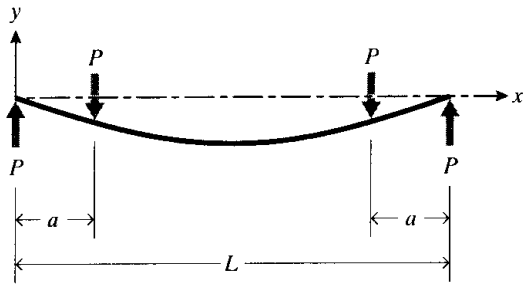

Figure I-1. Parameters of the four point bend test are *L*, the length of the beam, *P*, the applied load and *a*, the distance from the end of the beam of the load application point. In this experiment, the loads in the +y direction are the reaction forces from the supports and the -y direction loads are half the magnitude of the overall applied load.

Beam theory states that when a beam is loaded as shown in Figure H-1, the deflection and load are related by

$$\delta(x)=\frac{P(L-a)}{6LEI}\left(\frac{L}{L-a}(x-a)^3-x^3+\left(L^2-a\right)^2 x\right)+\frac{Pa}{6LEI}\left(\frac{L}{a}\left(x-(L-a)\right)^3-x^3+\left(L^2-a^2\right)x\right) \quad (1I)$$

where δ is the deflection in the -y direction at a distance *x* from the end of the beam, *P*, *L*, and a are the parameters as shown in Fig. I-1, *E* is the elastic (flexure) modulus of the material and *I* is the second moment of area of the cross section of the beam. (Roylance, 2000) If the dimensions and spring rate, P/δ, are known, these equations can then be solved for E.

A section cut anywhere between the two applied loads and summation of moments about this point will show that the moment in the beam in this span is constant and equal to P·a. The stress at fracture, or rupture modulus, can then be found by the beam bending maximum stress formula

$$\sigma = \frac{Mc}{I} = \frac{P_{\max} ah}{2I} \tag{2I}$$

Method

The dimensional values for the test specimens and fixture were as follows

L = 195.3mm

a = 50.0mm

b = 50.8mm

h = 8.9mm

Force was measured with a load cell style strain gage and deflection was measured with a linear variable differential transducer (LVDT). Force was applied by a piston that lifted the fixture. The test set up is shown in Fig. I-2.

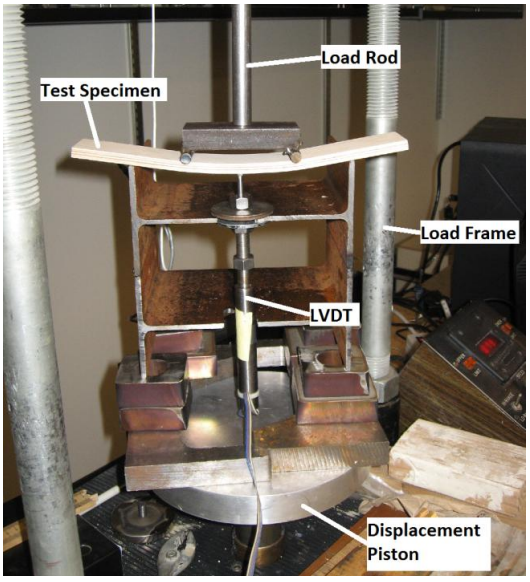

Figure I-2. The test apparatus was a compressive load frame with a fixture fabricated by the team. Not shown is the load cell (strain gauge) at the top of the load rod that attaches it to the frame and measures applied force.

The data acquisition system was a National Instruments LabView VI program that logged the data into text files and the data was processed with MATLAB resulting in the plot in Fig. I-3.

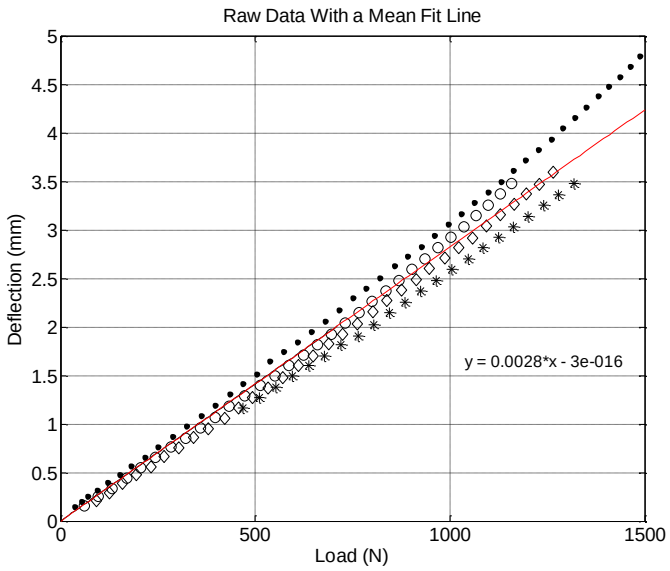

Figure I-3. Data was plotted and a mean fit line calculated by regression. The inverse of the slope of this line is F/□, the spring rate of the specimens, 3.54×10^5N/m.

Solving equation (1I) for E with x = L/2 and substituting the dimensional values yields

$$E = \frac{P}{\delta} 6.707 \times 10^4 \frac{1}{m} \tag{3I}$$

With P = F/2 since the total force was split between two load points, Eqn. 3I yields a flexure modulus of 11.88GPa (1.72Mpsi). The rupture modulus was calculated by Eqn. 2I with the lowest breaking load encountered to be 166MPa (24.1ksi).

[12.10] Appendix J: Roll-Over Speed Analysis

Introduction

This analysis provides the relation between rollover velocity (the velocity at which a rollover of the machine will occur) and corner radius. Some other constants, such as location of the center of gravity and the "track" width of the front end also contribute to the rollover velocity. By completing this analysis, the team will have quantified information that will allow for validation of certain design choices, like location of center of gravity, and track width. The team will also be able to verify results from previous HPV teams, and other sources to assure the team that the calculated results are within reason.

Given:

A free body diagram was created as shown in Fig. J-1, depicting the moments produced at the center of gravity about the contact patch of the tire. The forces are due to the weight of the rider and machine, and the radial force caused during cornering.

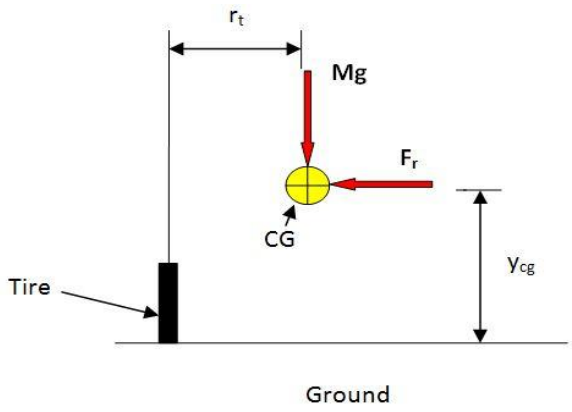

Figure J-1. Free-body diagram of moments involved in machine rollover analysis.

The force of the rider and machine, vertical distance to center of gravity, and half the track width are M = 250lbm, y_{cg} = 1.3ft, r_t = 1.1ft respectively.

Find:

The speed at which the machine will roll over in a 15ft radius turn

Solution:

By summing the moments and setting the equation equal to zero the following equation is produced:

$$\mathbf{F_r y_{cg} = Mgr_t} \tag{1J}$$

To get the radial force in terms of the corner radius the acceleration in the radial direction becomes:

$$\mathbf{a_r = \frac{v^2}{r_{corner}}} \tag{2J}$$

Substituting Equation 1J into Equation 2J and solving for velocity gives:

$$V_{roll}(r_{corner}) = \sqrt{\frac{32.2 * r_{corner} * r_t}{2 * y_{cg}}} * (\frac{3.6}{5.28}) \tag{3J}$$

This represents the relationship between the roll-over velocity and the corner radius given the stated parameters. Table J-1 below provides roll over velocities at different corner radii.

Table J-1. Roll over velocity vs. corner radius

r (ft)	V (mph)
10	7.95
11	8.34
12	8.71
13	9.07
14	9.41
15	9.74
16	10.06
17	10.37
18	10.67
19	10.96
20	11.25
21	11.53
22	11.80
23	12.06
24	12.32
25	12.58

Conclusion

The results are in an acceptable range when compared to previous HPV team's findings and intuitively are within reason for performance of an HPV. So, a track width of 26.4 inches and the location of the center of gravity will suffice. In testing, the performance of 2010 PSU HPV is comparable to the values calculated for rollover speed.

Note:

In testing it became evident that the initial track width was not adequate. The machine rolled over several times, and was easily put onto two wheels in cornering. When the front end was rebuilt, it was done so with a wider track width. This greatly mitigated the rollover problem, and the machine displayed greater stability and control.

[12.11] Appendix K: Bill of Materials

List of materials used in the construction and fabrication of the 2011 Human Powered Vehicle

Hardware

Item	Description	Quantity	Unit
Socket Cap Screw	M6 x 1.25	20	each
Socket Cap Screw	M8 x 1.00	10	each
Deep Groove Ball Bearing	6904-2RS1	4	each
Heim Joint	M8 x 1.25	2	each
Heim Joint	M6 x 1.00	2	each
Jam Nuts	M8 x 1.25	16	each
Nylon Lock Nuts	M6 x 1.00	14	each

Fairing Materials

Item	Description	Quantity	Unit
Mold	3" x 96" x 48 " foam	1	each
Fairing	9 sq yard Fiber glass 3k plain weave	1	each
Epoxy/Hardener	1 gal/0.25 gal	1	each

Stock Components

Part	Manufacturer	Quantity	Unit
Axle 110mm/20mm	Marzocchi	2	each
Rivel Crank Set 172.5mm 46/38	Sram	1	each
PC-951 Chain	Sram	3	each
Pit-Stop Break Cable Housing 5mm	Sram	2	each
Brake Cables	Jaguire	2	each
Disk Brake Kit 160mm	Avid BB-7	2	each
Rear Hub 500/14	Rohloff SpeedHub	1	each
Brake Lever	Avid	1	each
Rear Rim DA22 571mm BSD	Alex Rims	1	each
Rear Tire Race-light 25-571	Bontrager	1	each
Front Rim CR-18 349mm BSD	Sun/Ringlé	2	each
Front Tire Comet 37-349	Primo		
Idler	TerraCycle	2	each
Cane Creek Ten Headset	Cane Creek	1	each
Bottom Bracket Shell 1.5" OD x 68.5mm	Paragon Machine Works	1	each
Dropout: Rear, Horizontal, Relieved, 70 Degree	Paragon Machine Works	1	pair

Tubing

Item	Material	Wall Thickness/OD	Length	Unit
Roll-Bar	AISI 4130 steel	0.049"/1.5"	6'	each
Main Tube	AISI 4130 steel	0.049"/1.5"	4'	each
Crank Boom	AISI 4130 steel	0.049"/1.5"	2.5'	each
Chain Stay	AISI 4130 steel	0.049"/0.5"	3'	each
Seat Stay	AISI 4130 steel	0.049"/0.375"	3'	each
Supports	AISI 4130 steel	0.049"/1"	3.5'	each
Handle Bars	Al 6061 T6	0.049"/1"	4'	each
Head Block	Al 6061 T6	0.049"/2.25"	7"	each
Head Block	Al 6061 T6	0.049"/1"	30"	each

Raw Stock Material

Item	Material	Description	Quantity	Unit
Upright	Al 6061 T6	2" x 3.25" x 4" block	2	each
Hub	Al 6061 T6	4" x 3.5" cylinder	2	each
Seat Rail	Al 6061 T6	1.5" x 1.5" x 14" block	1	each
Head Block	Al 6061 T6	1.5" x 4" x 4" block	2	each
Wheel Mold	UHMW Plastic	1" x 24" x 36"	1	each
Carbon Fiber Wheels	Carbon Fiber Strips	2.5" x 17"	48	each
Carbon Fiber Wheels	Bulker Layer	0.25" x 16" x 16"	2	each
Carbon Fiber Wheels	Epoxy/Hardener	Marine Grade Tap	16 oz/8 oz	Each

[12.12] Appendix L: Maintenance Schedule

To maintain the safety and proper function of the vehicle, the following maintenance schedule should be followed.

Before Each Ride:

- Inspect tires (air pressure, sidewall and tread area for excessive wear or damage)
- Inspect brakes and cables
- Inspect crank set/drive-train components
- Inspect steering components for unobstructed movement
- Inspect frame for cracks

After Each Ride:

In addition to above:

- Clean, dry, and lubricate as necessary

Every Week or 100 miles or After Use in Wet Weather:

- In addition to above:
- Freewheel drive-train to ensure proper function and remove excess water
- Inspect/adjust/lubricate chain, derailleur, and disk brake sliders
- Inspect/adjust brake levers, cables, and calipers
- Inspect/adjust steering components
- Inspect wheel spoke/attachment tightness
- Lubricate all cables
- Inspect all hardware and re-torque as necessary
- Inspect joystick operation and handgrips

Every Month or 1000 miles:

In addition to above:

- Measure chain for wear

- Wax painted surfaces
- Treat wooden surfaces as necessary
- Inspect/Lubricate pedals and shoe cleats
- Grease bushings and tie-rod ends

Every Three Months or 3000 miles:

- In addition to above:
- Inspect frame joints for fatigue warnings
- Inspect/adjust bearings in crank set and head tubes
- Grease all metal/metal contact points
- Replace tires as necessary

Every Six Months or 6000 miles:

- In addition to above:
- Complete overhaul: disassembly, cleaning, and inspection
- Remove all cables and replace as necessary
- Replace all sealed bearings
- Replace brake pads as necessary

[12.13] Appendix M: Part Drawings

Engineering drawings of parts manufactured in house by the 2011 Human Power Vehicle Design Team.

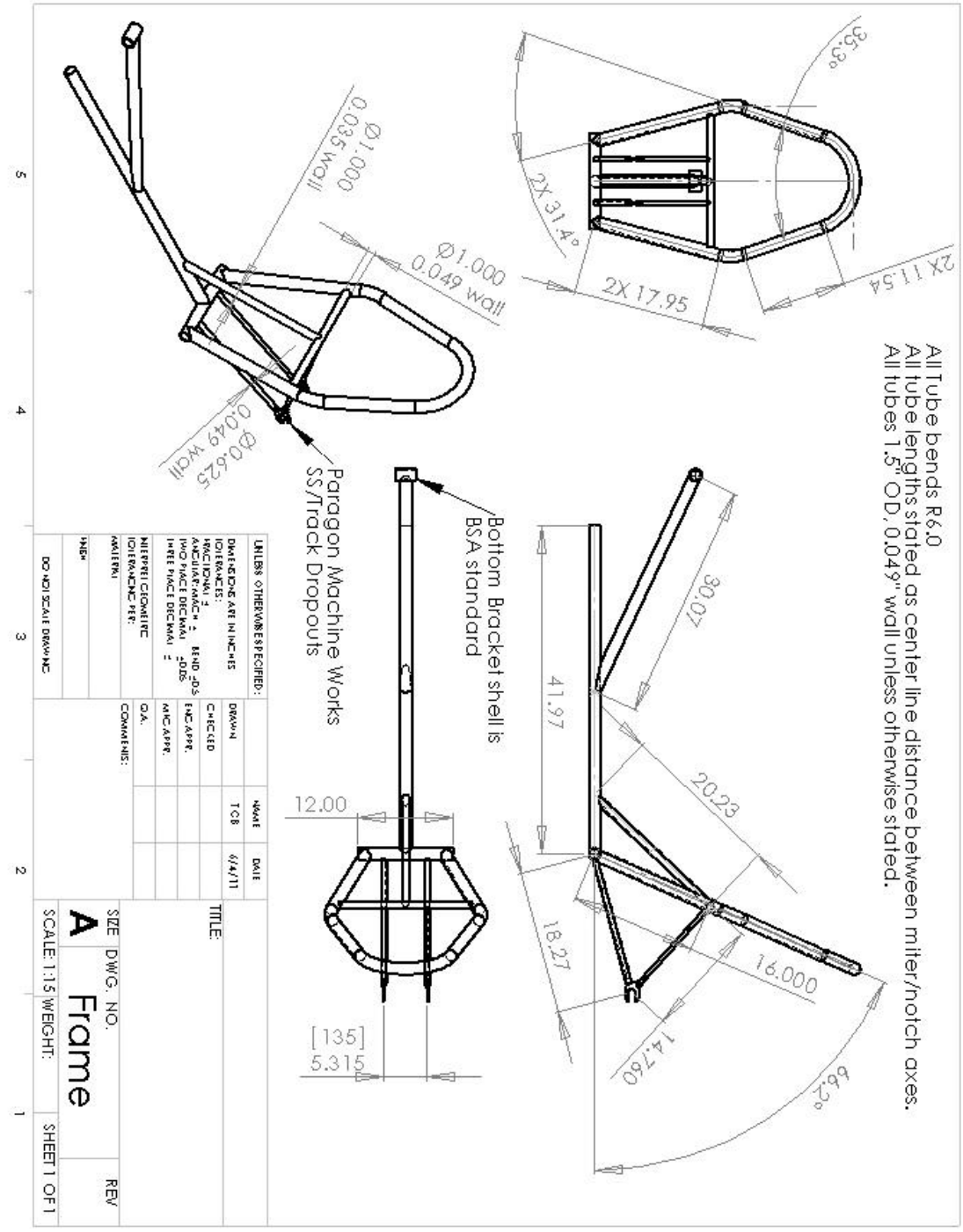

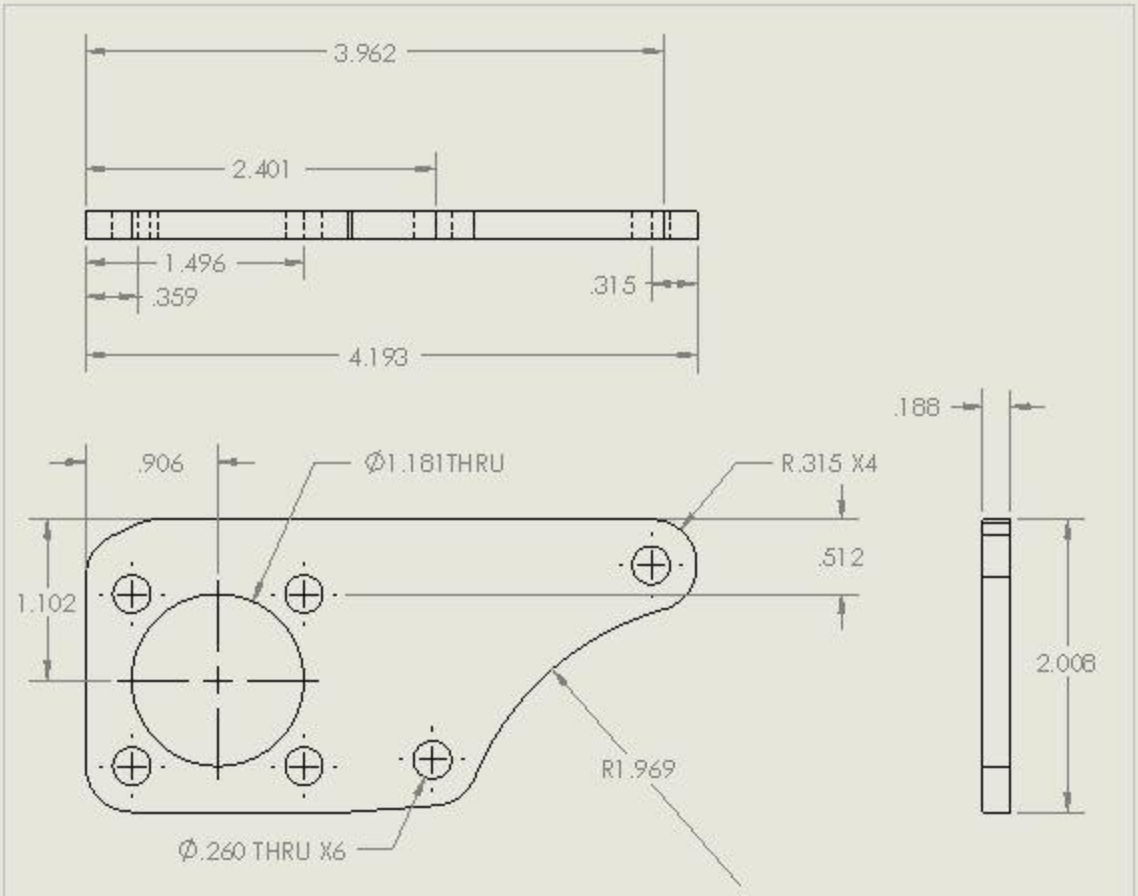

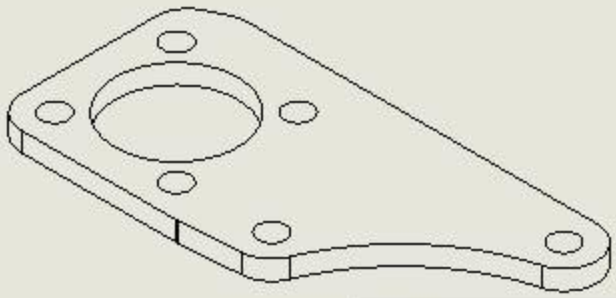

DIMENSIONS ARE IN INCHES TOLERANCES: FRACTIONAL ± ANGULAR: MACH ± BEND ± TWO PLACE DECIMAL ± THREE PLACE DECIMAL ±	TITLE: BREAK DISK TAB
	SIZE A — DWG. NO. DRAWING 6
MATERIAL: 6061 T6 ALUMINUM	
FINISH: NONE	SCALE:1:2 — SHEET 1 OF 1
DO NOT SCALE DRAWING	

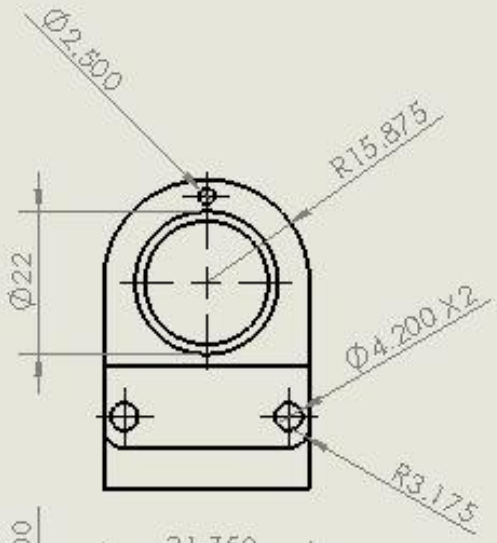

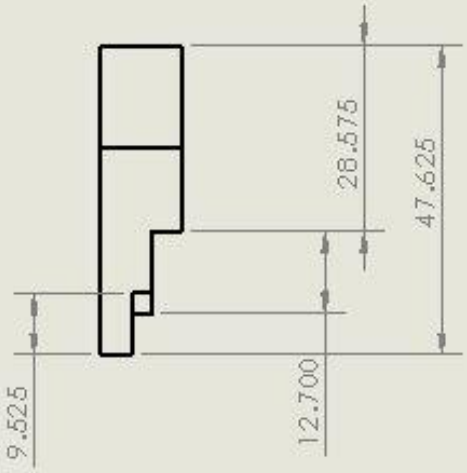

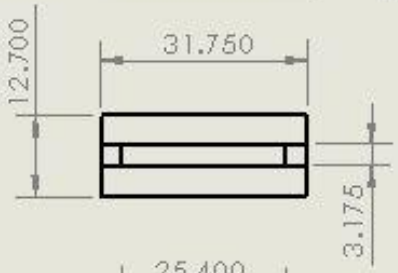

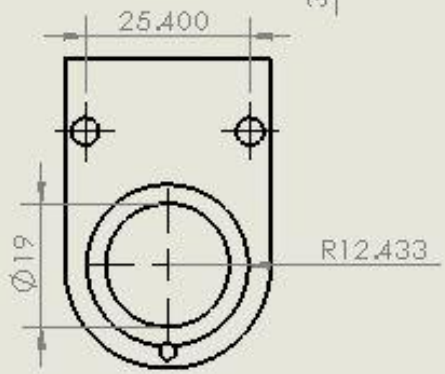

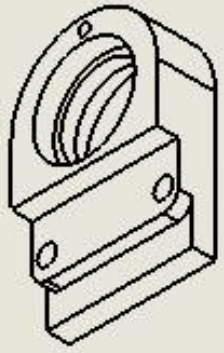

DIMENSIONS ARE IN MILLIMETERS TOLERANCES: FRACTIONAL ± ANGULAR: MACH ± BEND ± TWO PLACE DECIMAL ± THREE PLACE DECIMAL ±	TITLE: Bottom Pivot Carriers
	SIZE A — DWG. NO. DRAWING 2
MATERIAL: 6061 T6 ALUMINUM	
FINISH: NONE	SCALE:1:1 — SHEET 1 OF 1
DO NOT SCALE DRAWING	

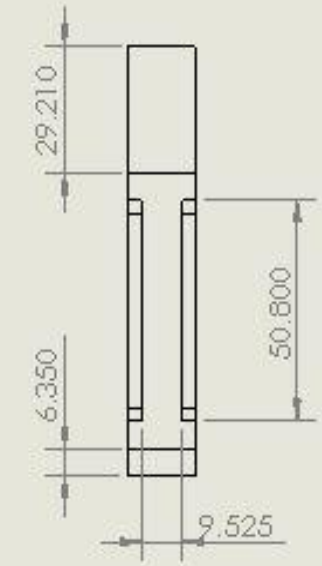

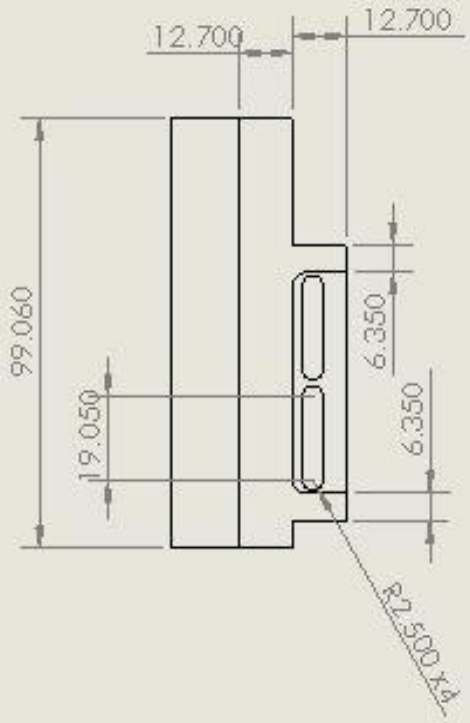

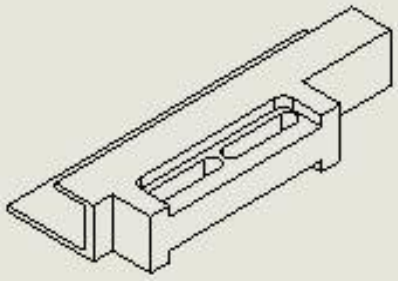

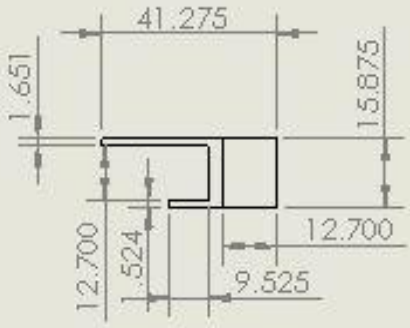

DIMENSIONS ARE IN MILLIMETERS TOLERANCES: FRACTIONAL ± ANGULAR: MACH ± BEND ± TWO PLACE DECIMAL ± THREE PLACE DECIMAL ±	TITLE: BOTTOM PLANK CAP
	SIZE A — DWG. NO. DRAWING 8
MATERIAL: 6061 T6 ALUMINUM	
FINISH: NONE	SCALE:1:2 — SHEET 1 OF 1
DO NOT SCALE DRAWING	

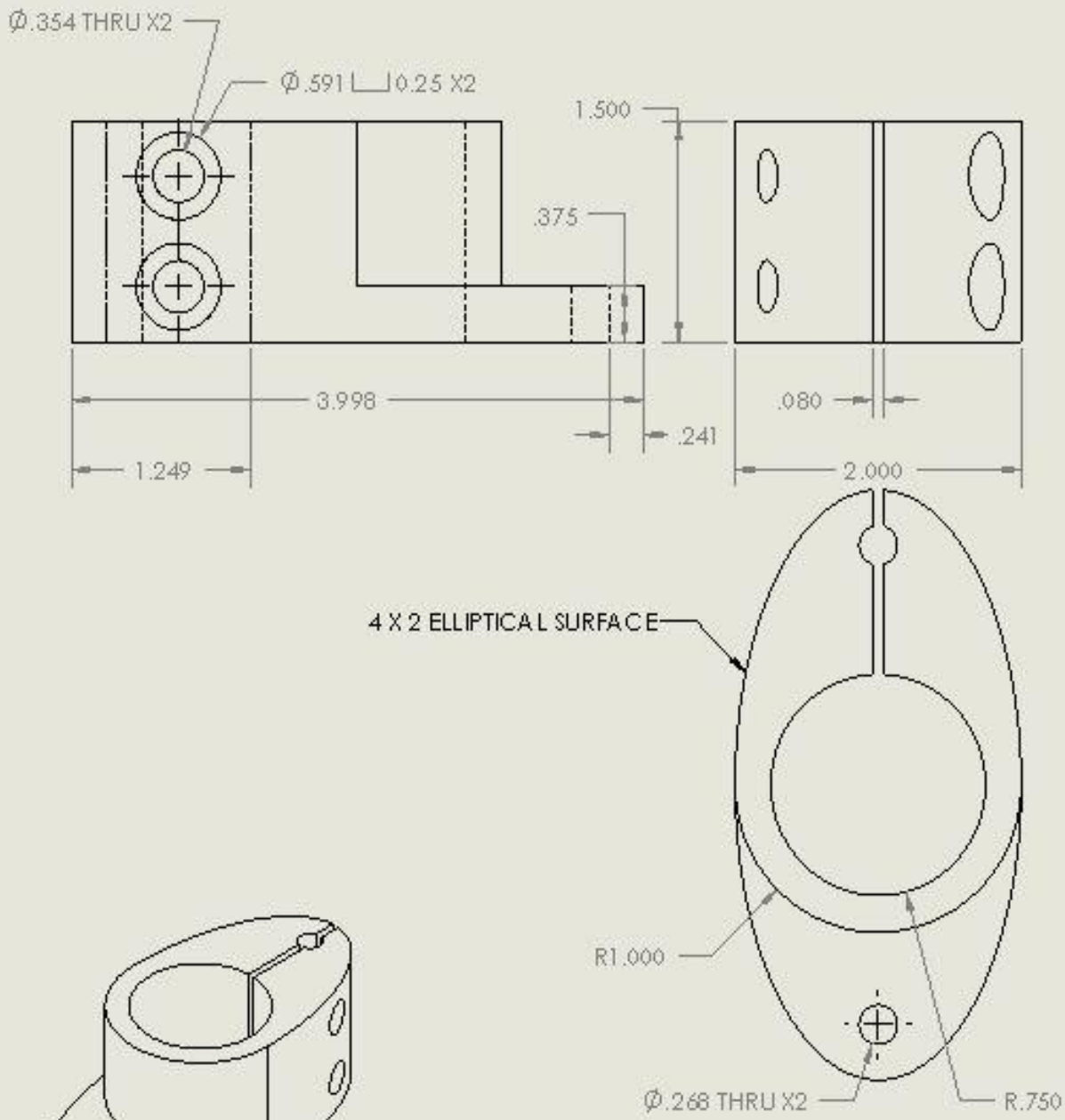

DIMENSIONS ARE IN INCHES TOLERANCES: FRACTIONAL ± ANGULAR: MACH ± BEND ± TWO PLACE DECIMAL ± THREE PLACE DECIMAL ±	TITLE: HS CLAMP
	SIZE A — DWG. NO. DRAWING 5
MATERIAL: 6061 T6 ALUMINUM	
FINISH: NONE	SCALE:1:2 — SHEET 1 OF 1
DO NOT SCALE DRAWING	

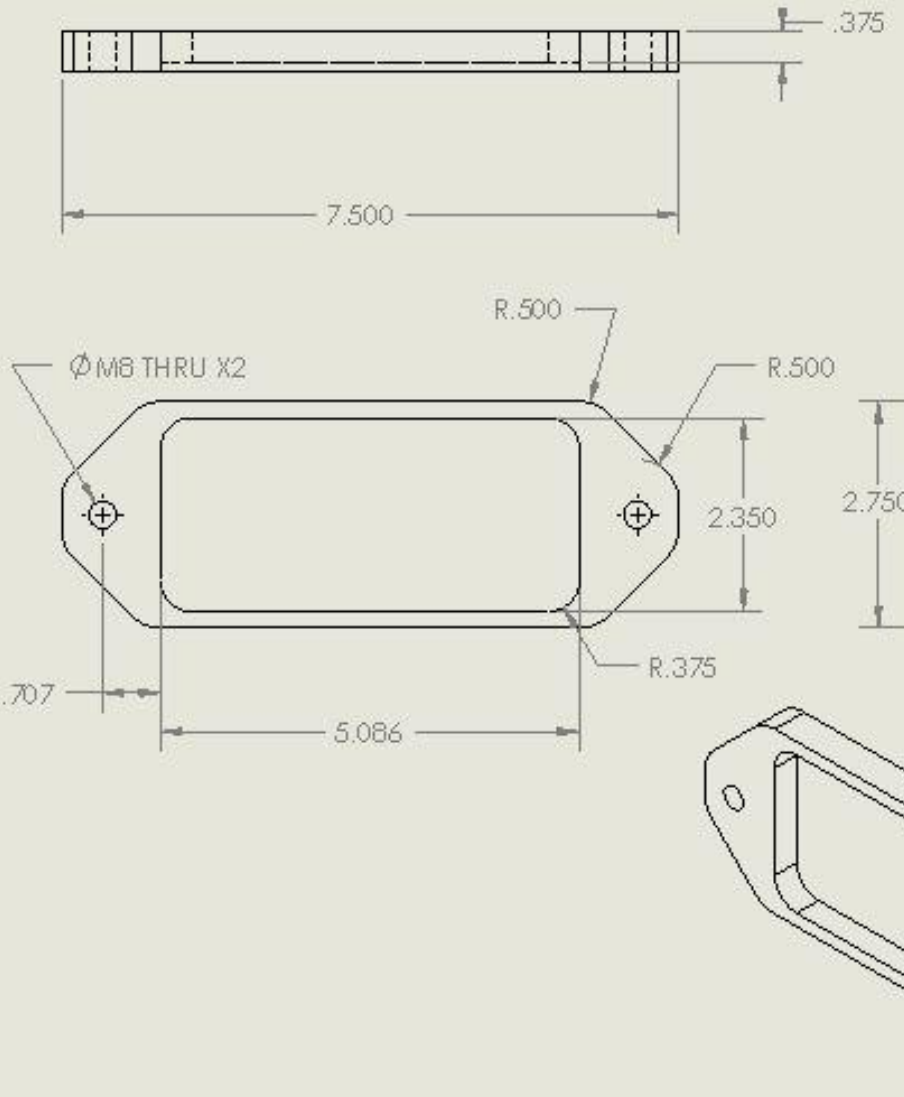

DIMENSIONS ARE IN INCHES TOLERANCES: FRACTIONAL ± ANGULAR: MACH ± BEND ± TWO PLACE DECIMAL ± THREE PLACE DECIMAL ±	TITLE: CLAMP PLATE
	SIZE A — DWG. NO. DRAWING 4
MATERIAL: 6061 T6 ALUMINUM	
FINISH: NONE	SCALE:1:2 — SHEET 1 OF 1
DO NOT SCALE DRAWING	

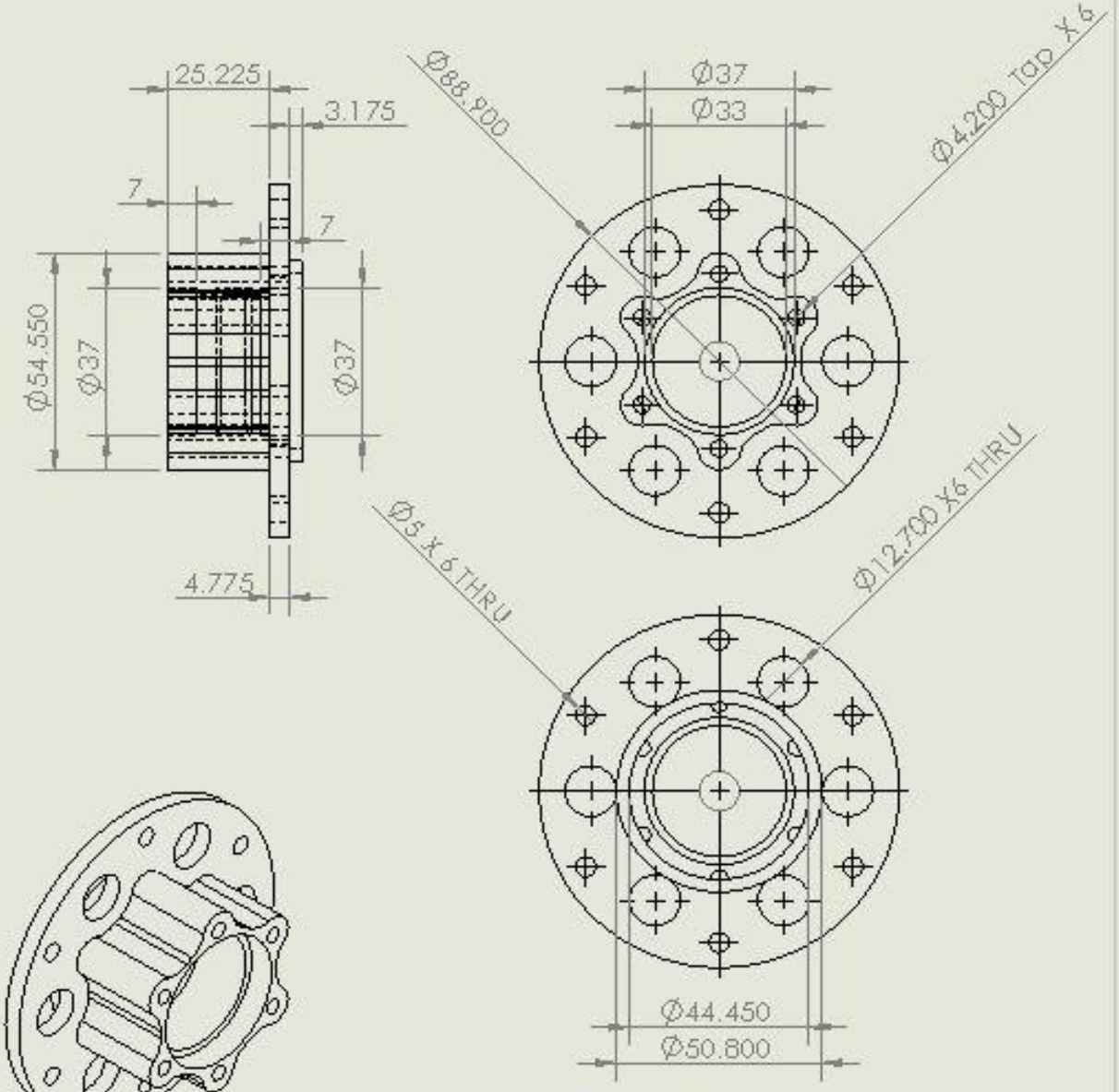

DIMENSIONS ARE IN MILLIMETERS TOLERANCES: FRACTIONAL ± ANGULAR: MACH ± BEND ± TWO PLACE DECIMAL ± THREE PLACE DECIMAL ±	TITLE: HUB
MATERIAL: 6061 T6 ALUMINUM	SIZE A — DWG. NO. DRAWING 1
FINISH: NONE	SCALE:1:2 — SHEET 1 OF 1
DO NOT SCALE DRAWING	

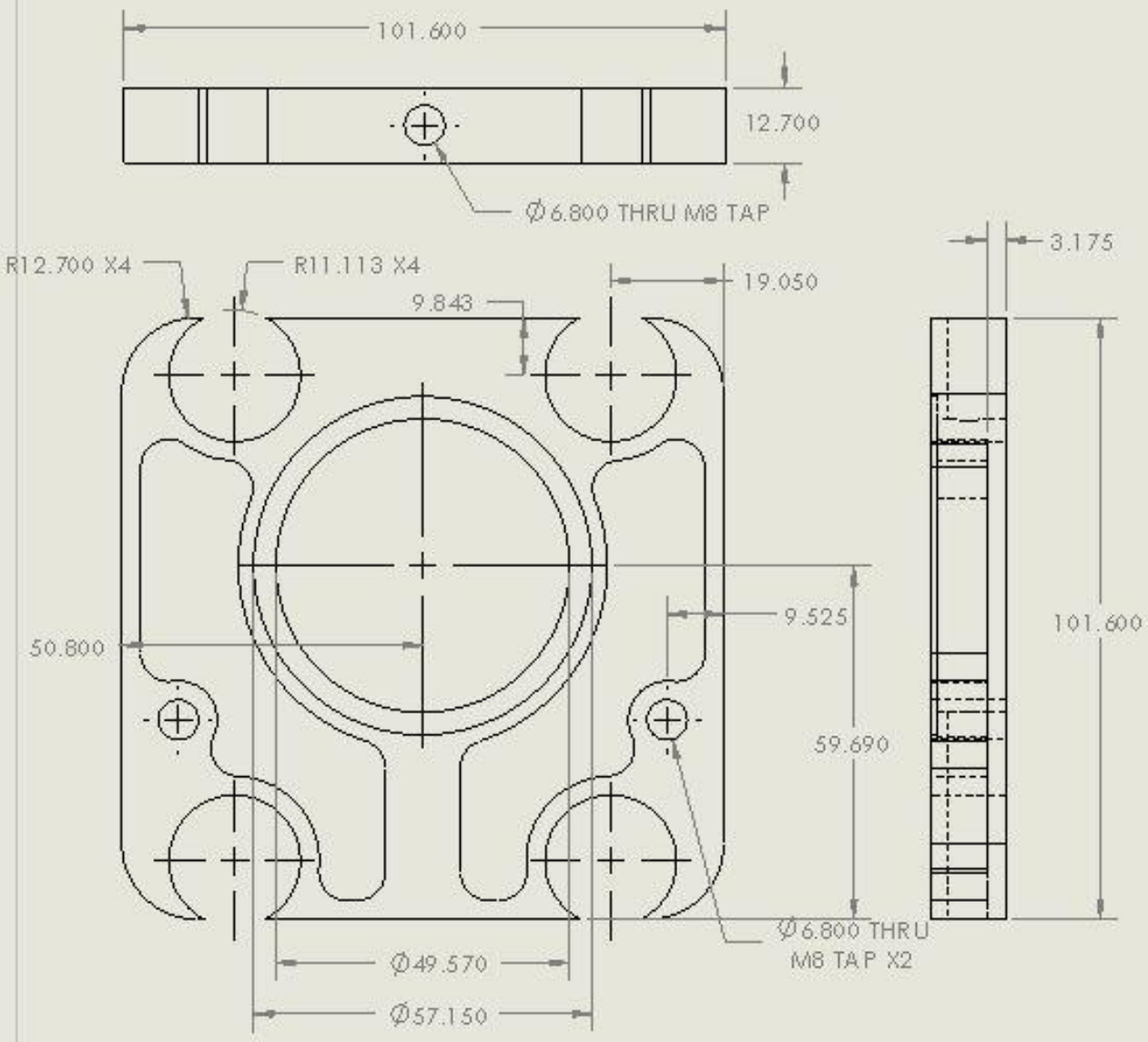

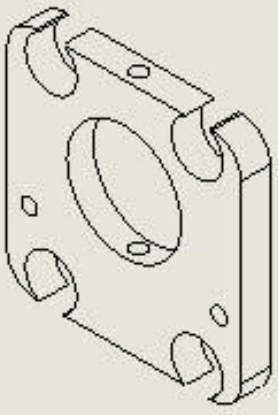

DIMENSIONS ARE IN MILLIMETERS TOLERANCES: FRACTIONAL ± ANGULAR: MACH ± BEND ± TWO PLACE DECIMAL ± THREE PLACE DECIMAL ±	TITLE: MAIN PIVOT PLATE
MATERIAL: 6061 T6 ALUMINUM	SIZE A — DWG. NO. DRAWING 7
FINISH: NONE	SCALE:1:1 — SHEET 1 OF 1
DO NOT SCALE DRAWING	

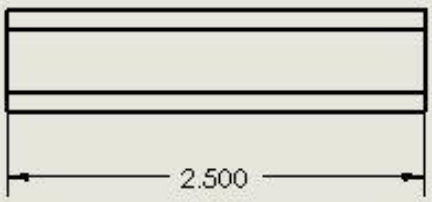

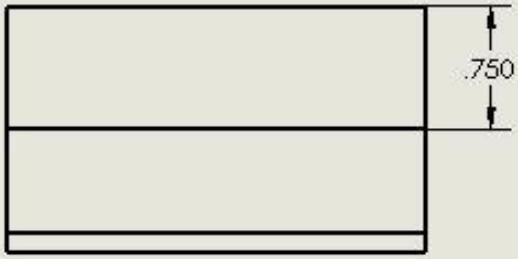

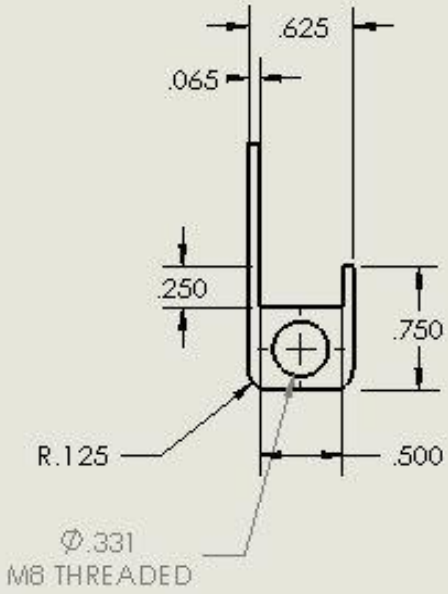

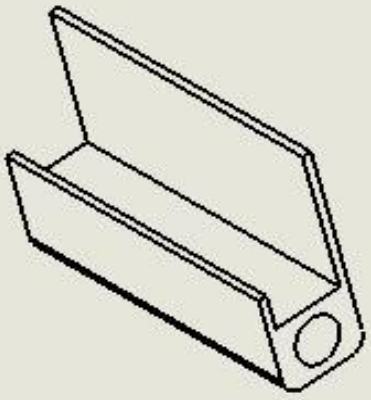

DIMENSIONS ARE IN INCHES TOLERANCES: FRACTIONAL ± ANGULAR: MACH ± BEND ± TWO PLACE DECIMAL ± THREE PLACE DECIMAL ±	TITLE: TOP PIVOT MOUNT
MATERIAL: 6061 T6 ALUMINUM	SIZE A — DWG. NO. DRAWING 3
FINISH: NONE	SCALE:1:1 — SHEET 1 OF 1
DO NOT SCALE DRAWING	

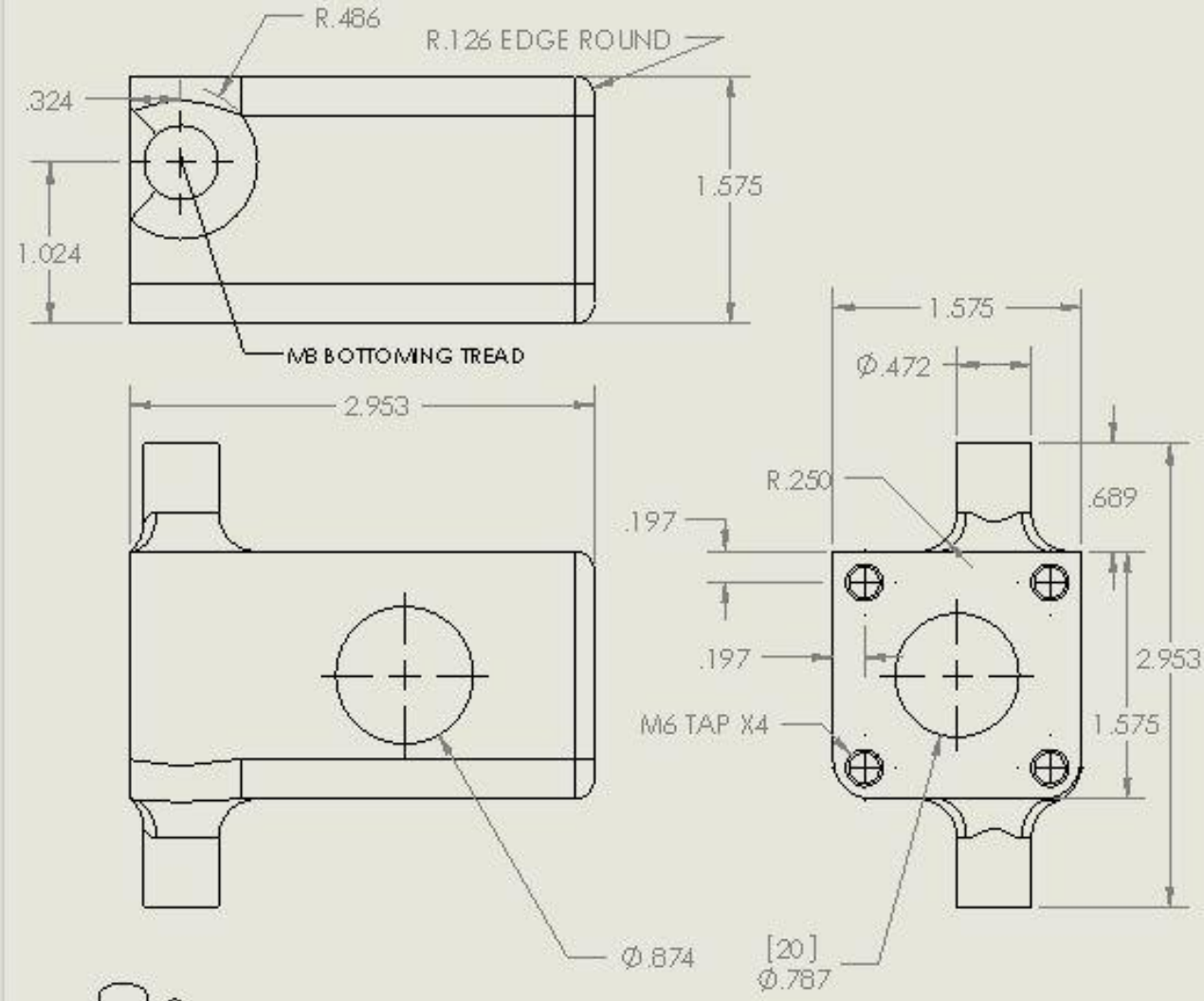

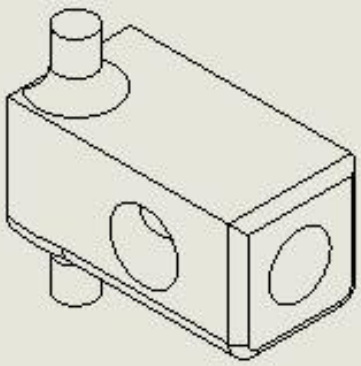

DIMENSIONS ARE IN INCHES TOLERANCES: FRACTIONAL ± ANGULAR: MACH ± BEND ± TWO PLACE DECIMAL ± THREE PLACE DECIMAL ±	TITLE: UPRIGHT
MATERIAL: 6061 T6 ALUMINUM	SIZE A DWG. NO. DRAWING 9
FINISH: NONE	SCALE:1:1 SHEET 1 OF 1
DO NOT SCALE DRAWING	

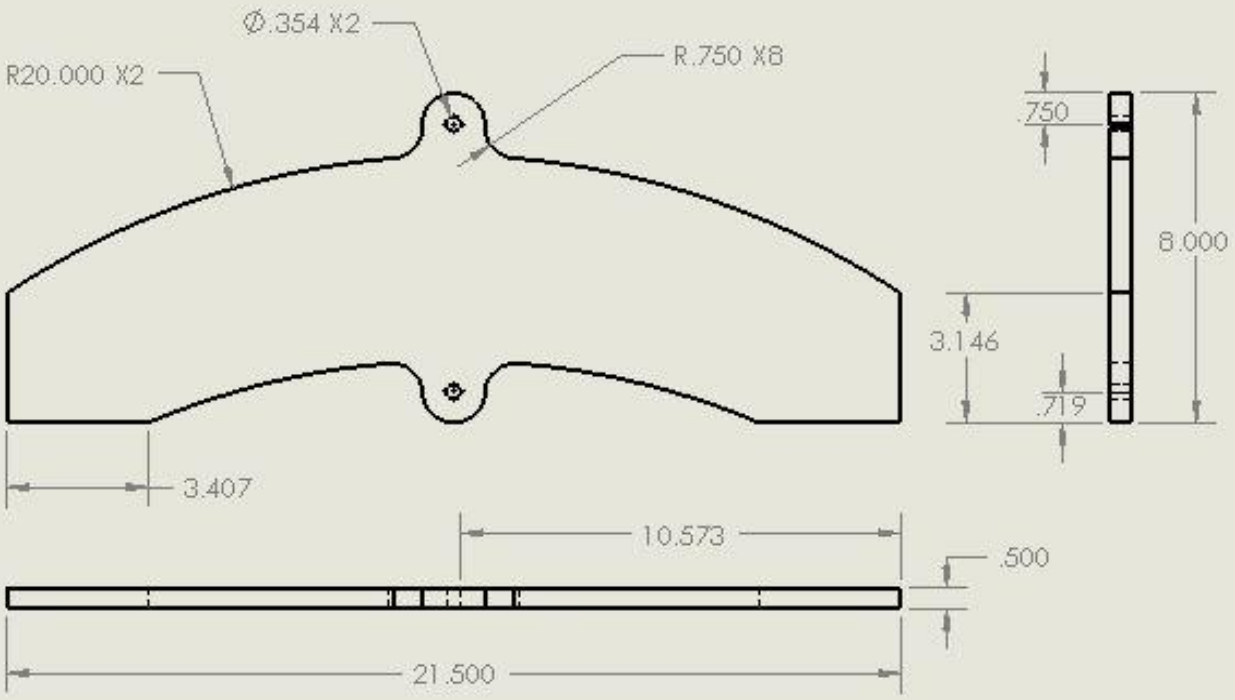

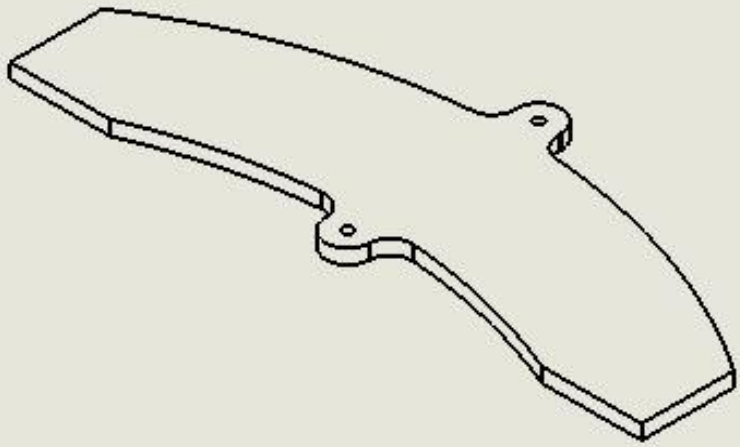

DIMENSIONS ARE IN INCHES TOLERANCES: FRACTIONAL ± ANGULAR: MACH ± BEND ± TWO PLACE DECIMAL ± THREE PLACE DECIMAL ±	TITLE: TOP CROSS MEMBER
	SIZE A — DWG. NO. DRAWING 10
MATERIAL: BALTIC BIRCH	
FINISH: NONE	SCALE:1:8 — SHEET 1 OF 1
DO NOT SCALE DRAWING	

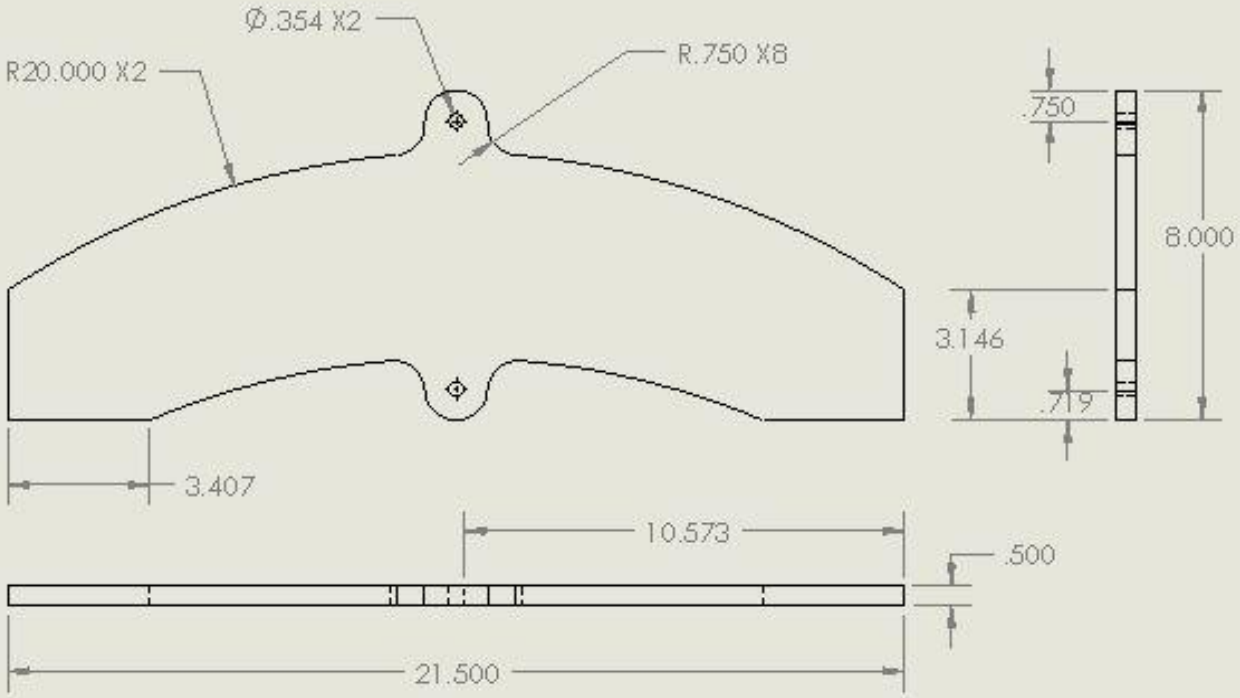

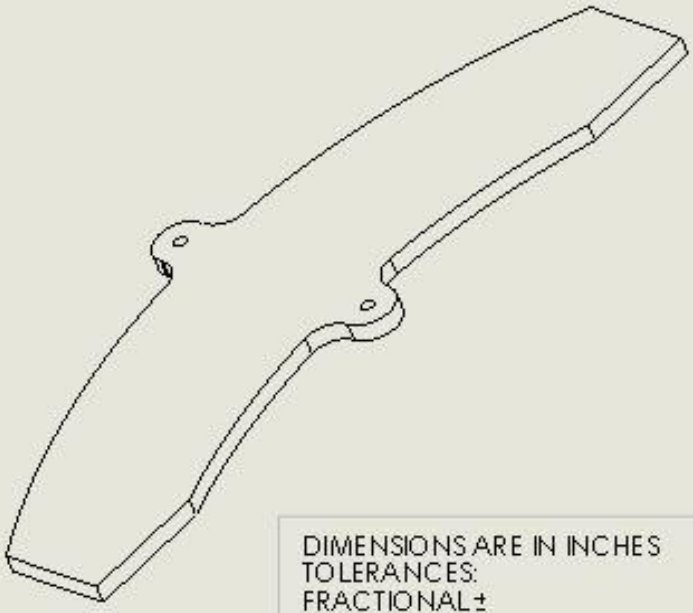

DIMENSIONS ARE IN INCHES TOLERANCES: FRACTIONAL ± ANGULAR: MACH ± BEND ± TWO PLACE DECIMAL ± THREE PLACE DECIMAL ±	TITLE: BOTTOM CROSS MEMBER
MATERIAL: BALTIC BIRCH	SIZE A — DWG. NO. DRAWING 11
FINISH: NONE	SCALE:1:8 — SHEET 1 OF 1
DO NOT SCALE DRAWING	

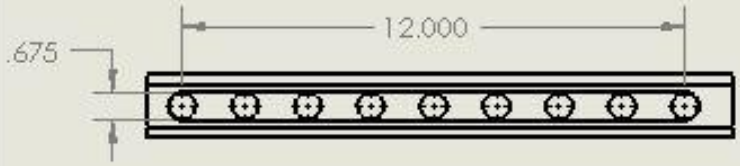

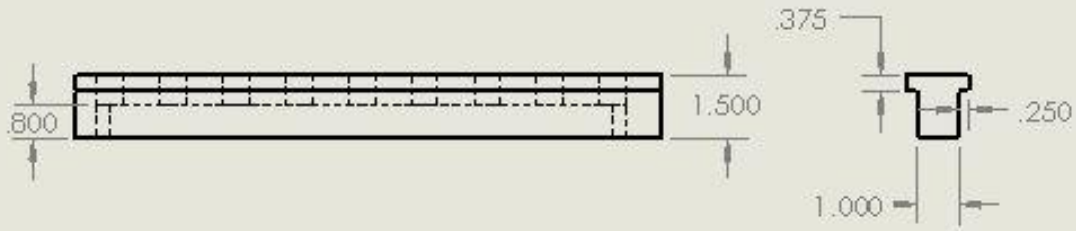

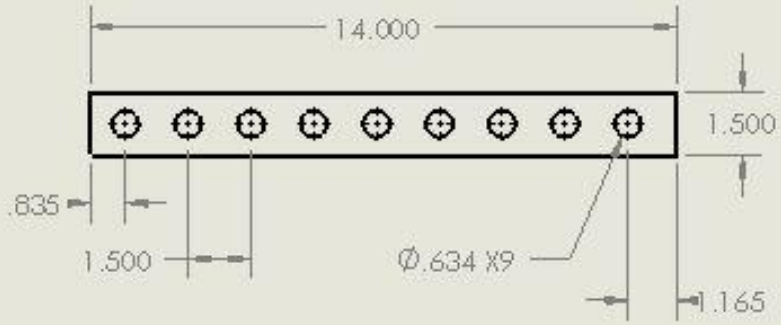

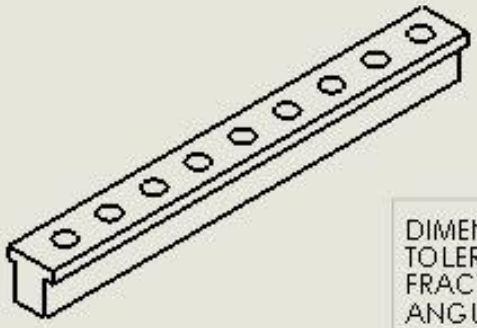

DIMENSIONS ARE IN INCHES TOLERANCES: FRACTIONAL ± ANGULAR: MACH ± BEND ± TWO PLACE DECIMAL ± THREE PLACE DECIMAL ±	TITLE: SEAT RAIL
	SIZE A DWG. NO. DRAWING 12
MATERIAL: 6061 T6 ALUMINUM	
FINISH: NONE	SCALE: 1:4 SHEET 1 OF 1
DO NOT SCALE DRAWING	

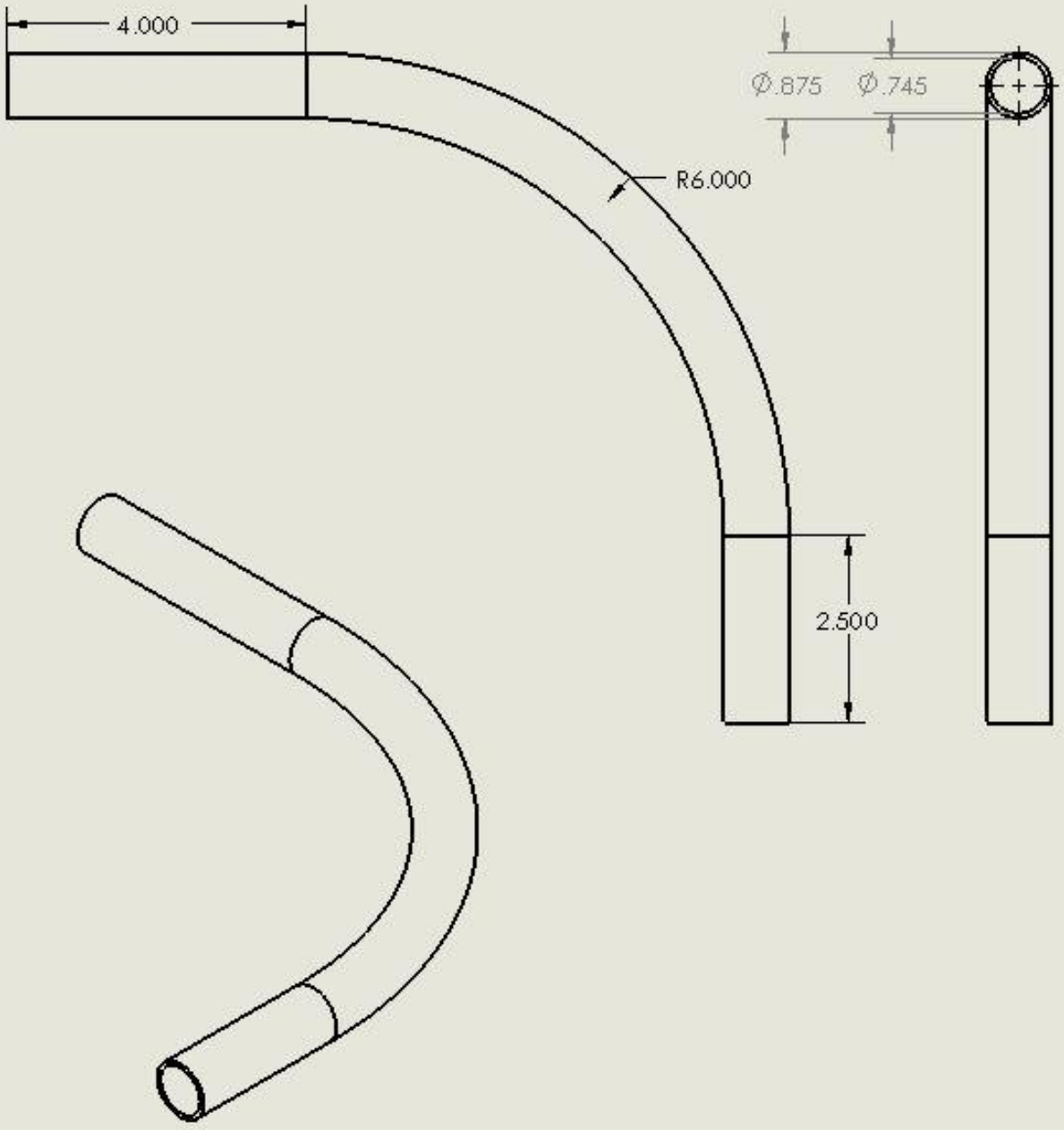

DIMENSIONS ARE IN INCHES TOLERANCES: FRACTIONAL ± ANGULAR: MACH ± BEND ± TWO PLACE DECIMAL ± THREE PLACE DECIMAL ±	TITLE: HANDLEBAR
	SIZE A DWG. NO. DRAWING 13
MATERIAL: 6061 T6 ALUMINUM	
FINISH: NONE	SCALE: 1:2 SHEET 1 OF 1
DO NOT SCALE DRAWING	

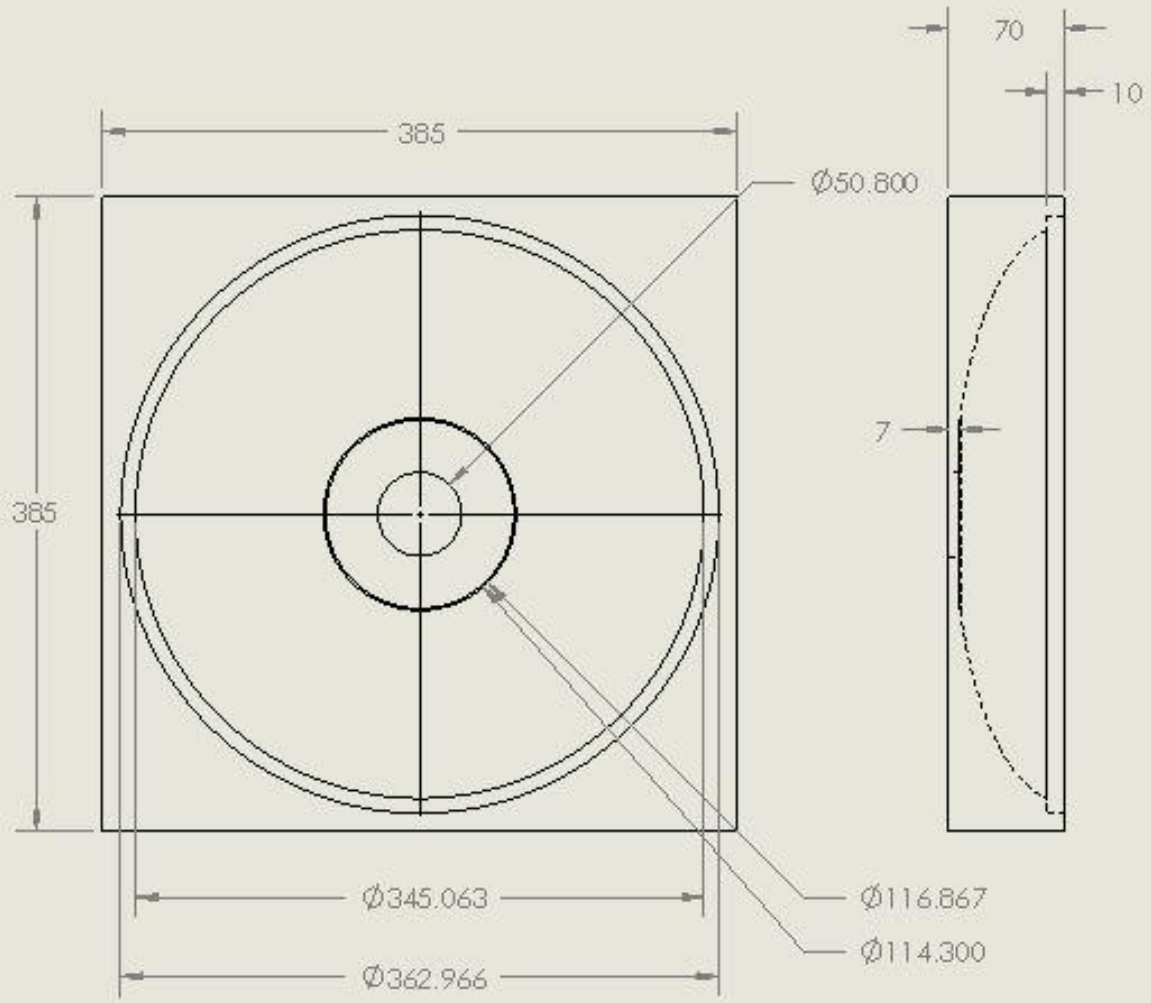

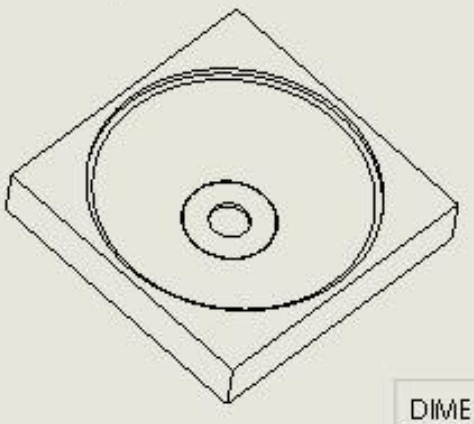

DIMENSIONS ARE IN MILLIMETERS TOLERANCES: FRACTIONAL ± ANGULAR: MACH ± BEND ± TWO PLACE DECIMAL ± THREE PLACE DECIMAL ±	TITLE: WHEEL MOLD
	SIZE A · DWG. NO. DRAWING 14
MATERIAL: UHMW POLYETHYLENE	
FINISH: NONE	SCALE: 1:4 · SHEET 1 OF 1
DO NOT SCALE DRAWING	

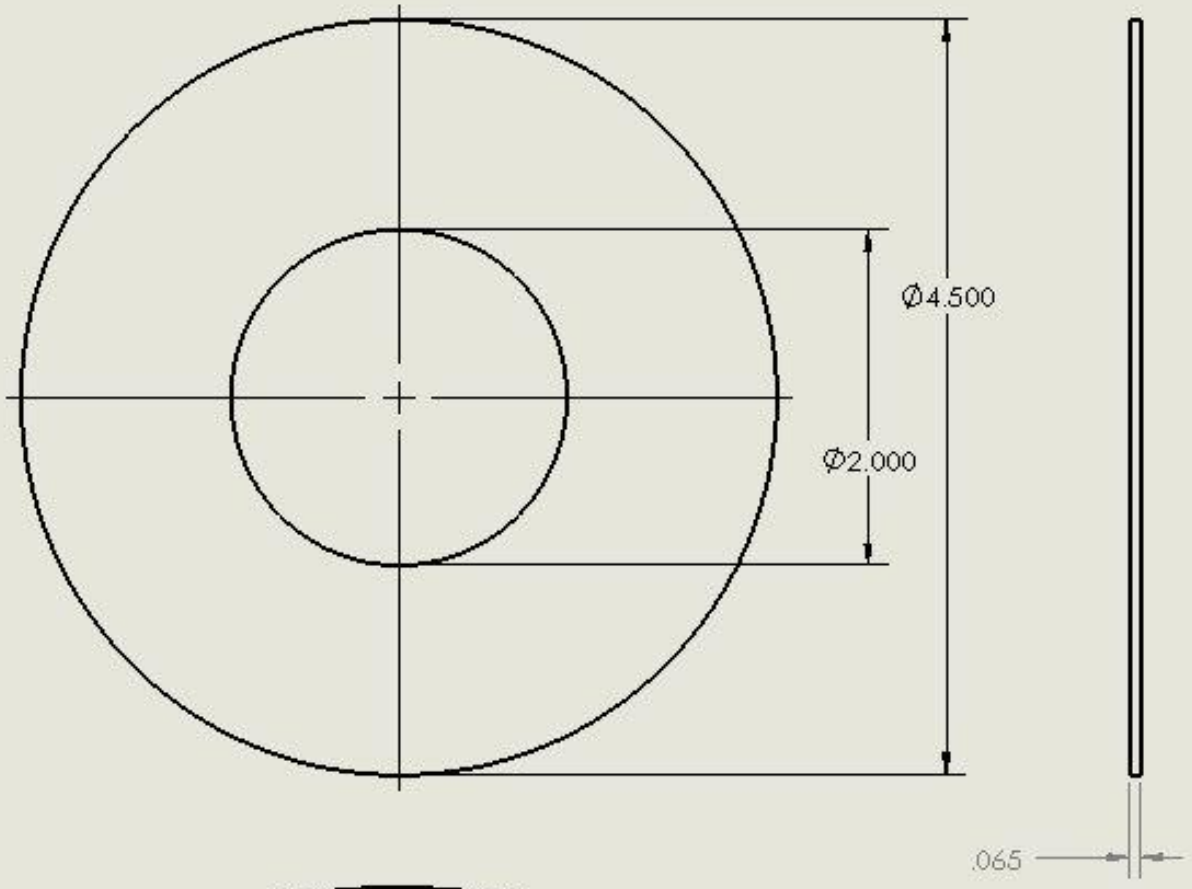

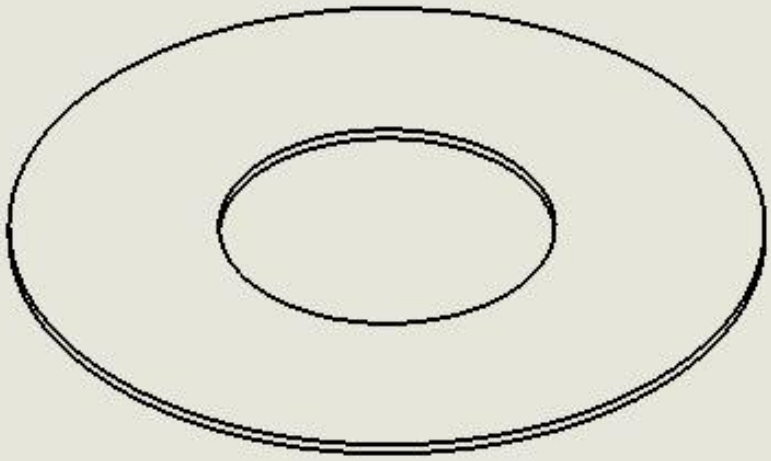

DIMENSIONS ARE IN INCHES TOLERANCES: FRACTIONAL ± ANGULAR: MACH ± BEND ± TWO PLACE DECIMAL ± THREE PLACE DECIMAL ±	TITLE: WHEEL SUPPORT RING
MATERIAL: 6061 T6 ALUMINUM	SIZE A — DWG. NO. DRAWING 15
FINISH: NONE	SCALE: 1:1 — SHEET 1 OF 1
DO NOT SCALE DRAWING	

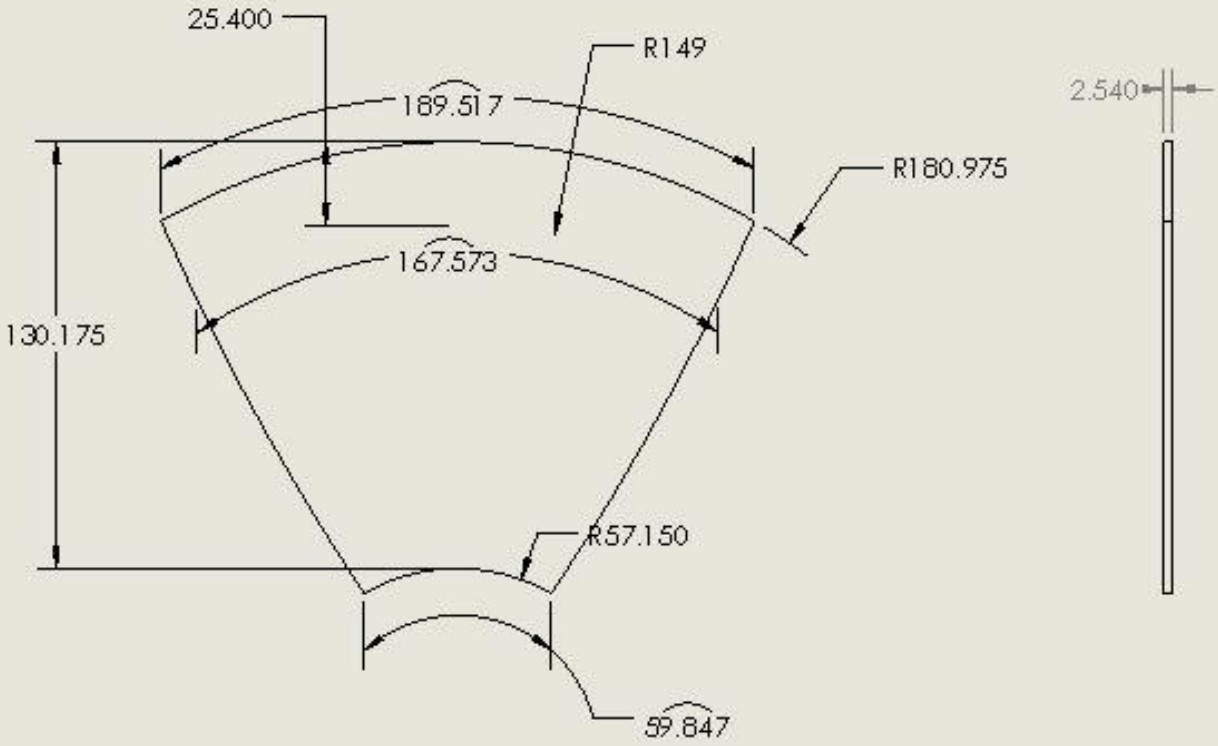

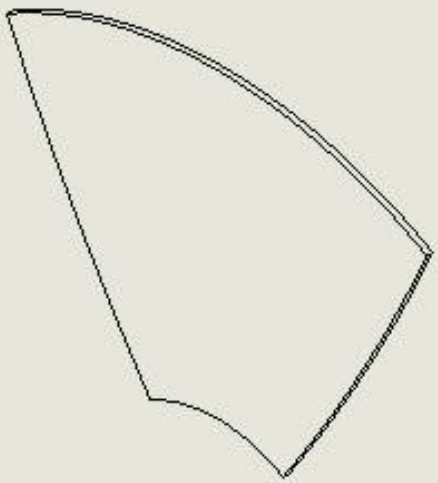

DIMENSIONS ARE IN MILLIMETERS TOLERANCES: FRACTIONAL ± ANGULAR: MACH ± BEND ± TWO PLACE DECIMAL ± THREE PLACE DECIMAL ±	TITLE: WHEEL BULKER LAYER
	SIZE A DWG. NO. DRAWING 16
MATERIAL: COREMAT	
FINISH: NONE	SCALE:1:2 SHEET 1 OF 1
DO NOT SCALE DRAWING	

Exploded view of the carbon fiber hub centered wheel showing internal layers and layup process order

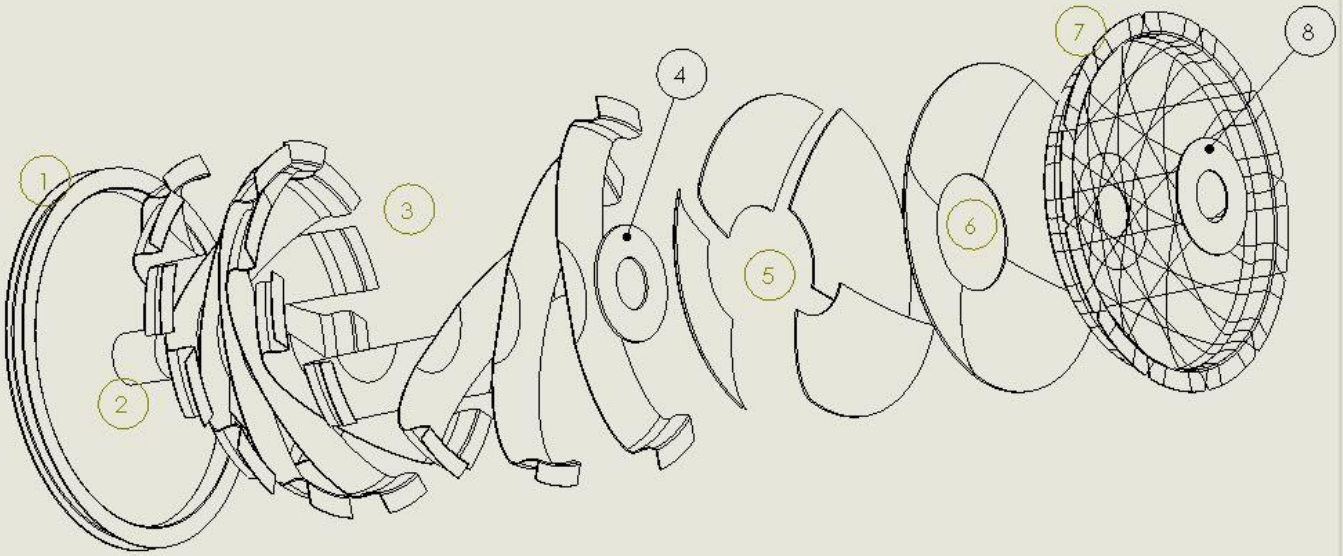

1. Rim
2. Centering Block
3. First Carbon Strip Layer, Exploded
4. Internal Hub Plate
5. First Bulker Layer, Exploded
6. Second bulker layer
7. Second Carbon Strip Layer
8. External Hub Face Plate

Part Layup into the mold in numbered order. All aluminum parts to be rough sanded and epoxy coated prior to layup. Centering block is 2" delrin or UHMW plastic round stock to centerthe hub plates in the rim and is removed after epoxy cure

5 4 3 2 1

[13] References

ASME. (2011). *Human Powered Vehicle Challenge*. Retrieved March 7, 2011, from http://www.asme.org/Events/Contests/HPV/Human_Powered_Vehicle.cfm

Forest Products Laboratory. (1999). *Wood Handbook, Wood as an Engineering Material.* Madison: United Strates Departemnt of Agriculture.

Frank P. Incropera, D. P. (2007). *Fundamentals of Heat and Mass Transfer.* Hoboken, New Jersey: John Wiley & Sons Inc.

Local Climate Data from Portland Airport. (2009, June). Retrieved April 11, 2011, from National Weather Service: http://www.wrh.noaa.gov/pqr/pdxclimate/index.php

Raul F. Reiser II, M. L. (2001). Anaerobic Cycling Power Output with Variations in Recumbent Body Configuration. *Journal of Applied Biomechanics* .

Roylance, D. (2000, November 30). *3.11 Mechanics of Materials Fall 2000.* Retrieved April 2, 2011, from MIT Open Courseware: http://ocw.mit.edu/courses/materials-science-and-engineering/3-11-mechanics-of-materials-fall-1999/modules/bdisp.pdf

Thomas, R. (2009). *BTA: Legal Resources.* Retrieved April 2, 2011, from Bicycle Transportation Alliance: http://www.stc-law.com/pdf/PP7thEdition.pdf

Wianecki, R. (2002, March 26). *Rick Wianecki's Leaning Trike Project*. Retrieved March 6, 2011, from http://www.recumbents.com/wisil/wianecki/leaning_trike3.htm

Wilson, David Gordon; Jim Papadopoulos (2004). Bicycling Science (Third ed.). The MIT Press. p. 126. ISBN 0-262-73154-1. "aerodynamic drag force is proportional to the square of the velocity"

Cengel, Yunus A.; Michael A. Boles (2008). Thermodynamics: An engineering approach (Sixth ed.) McGraw-Hill. p. 83.